2020-05-22

# Long-term thermal sensitivity of Earth's tropical forests

## Sullivan, MJP

http://hdl.handle.net/10026.1/15706

# Long-term thermal sensitivity of Earth's tropical forests

Martin J. P. Sullivan[1,2], Simon L. Lewis[1,3], Kofi Affum-Baffoe[4], Carolina Castilho[5], Flávia Costa[6], Aida Cuni Sanchez[7,8], Corneille E. N. Ewango[9,10,11], Wannes Hubau[1,12,13], Beatriz Marimon[14], Abel Monteagudo-Mendoza[15], Lan Qie[16], Bonaventure Sonké[17], Rodolfo Vasquez Martinez[15], Timothy R Baker[1], Roel J. W. Brienen[1], Ted R. Feldpausch[18], David Galbraith[1], Manuel Gloor[1], Yadvinder Malhi[19], Shin-Ichiro Aiba[20], Miguel N. Alexiades[21], Everton C. Almeida[22], Edmar Almeida de Oliveira[23], Esteban Álvarez Dávila[24], Patricia Alvarez Loayza[25], Ana Andrade[26], Simone Aparecida Vieira[27], Luiz Aragão[28], Alejandro Araujo-Murakami[29], Eric J.M.M. Arets[30], Luzmila Arroyo[31], Peter Ashton[32], Gerardo Aymard C.[33], Fabrício B. Baccaro[34], Lindsay F. Banin[35], Christopher Baraloto[36], Plínio Barbosa Camargo[37], Jos Barlow[38], Jorcely Barroso[39], Jean-François Bastin[40], Sarah A. Batterman[1,41,42,43], Hans Beeckman[12], Serge K. Begne[17,44], Amy C. Bennett[44], Erika Berenguer[19,38], Nicholas Berry[45], Lilian Blanc[46], Pascal Boeckx[47], Jan Bogaert[48], Damien Bonal[49], Frans Bongers[50], Matt Bradford[51], Francis Q. Brearley[2], Terry Brncic[52], Foster Brown[53], Benoit Burban[54], José Luís Camargo[26], Wendeson Castro[55], Carlos Céron[56], Sabina Cerruto Ribeiro[57], Victor Chama Moscoso[15], Jerôme Chave[58], Eric Chezeaux[59], Connie J. Clark[25], Fernanda Coelho[1], Murray Collins[61], James A. Comiskey[62,63], Fernando Cornejo Valverde[64], Massiel Corrales Medina[65], Lola da Costa[66], Martin Dančák[67], Greta C. Dargie[1], Stuart Davies[68], Nallaret Davila Cardozo[69], Thales de Haulleville[12,48], Marcelo Brilhante de Medeiros[70], Jhon del Aguila Pasquel[71], Géraldine Derroire[72], Anthony Di Fiore[73], Jean-Louis Doucet[74], Aurélie Dourdain[72], Vincent Droissant[75], Luisa Fernanda Duque[76], Romeo Ekoungoulou[77], Fernando Elias[78], Terry Erwin[79], Adriane Esquivel-Muelbert[80], Sophie Fauset[81], Joice Ferreira[82], Gerardo Flores Llampazo[83], Ernest Foli[84], Andrew Ford[51], Martin Gilpin[1], Jefferson S. Hall[85], Keith C. Hamer[86], Alan C. Hamilton[87], David J. Harris[88], Terese B. Hart[89,90], Radim Hédl[91,92], Bruno Herault[72], Rafael Herrera[93], Niro Higuchi[6], Annette Hladik[94], Eurídice Honorio Coronado[71], Isau Huamantupa-Chuquimaco[95], Walter Huaraca Huasco[95], Kathryn J. Jeffery[96], Eliana Jimenez-Rojas[97], Michelle Kalamandeen[1], Marie-Noel Kamdem[11,13,17,98], Elizabeth Kearsley[99], Ricardo Keichi Umetsu[100], Lip Khoon Kho[101], Timothy Killeen[102], Kanehiro Kitayama[103], Bente Klitgaard[104], Alexander Koch[105], Nicolas Labrière[58], William Laurance[106], Susan Laurance[106], Miguel E. Leal[107], Aurora Levesley[1], Adriano J. N. Lima[6], Janvier Lisingo[11], Aline P. Lopes[108,109], Gabriela Lopez-Gonzalez[1], Tom Lovejoy[110], Jon Lovett[1], Richard Lowe[111], William E. Magnusson[112], Jagoba Malumbres-Olarte[113,114], Ângelo Gilberto Manzatto[115], Ben Hur Marimon Junior[116], Andrew R. Marshall[8,117,118], Toby Marthews[119], Simone Matias de Almeida Reis[14,19], Colin Maycock[120], Karina Melgaço[1], Casimiro Mendoza[121], Faizah Metali[122], Vianet Mihindou[123,124], William Milliken[104], Edward Mitchard[125], Paulo S. Morandi[14], Hannah L. Mossman[2], Laszlo Nagy[126], Henrique Nascimento[6], David Neill[127], Reuben Nilus[128], Percy Núñez Vargas[95], Walter Palacios[129], Nadir Pallqui Camacho[1,95], Julie Peacock[1], Colin Pendry[130], Maria Cristina Peñuela Mora[131], Georgia C. Pickavance[1], John Pipoly[132], Nigel Pitman[133], Maureen Playfair[134], Lourens Poorter[135], John R. Poulsen[25], Axel D. Poulsen[136], Richard Preziosi[2], Adriana Prieto[137], Richard Primack[138], Hirma Ramírez-Angulo[139], Jan Reitsma[140], Maxime Réjou-Méchain[75], Zorayda Restrepo Correa[141], Thaiane Rodrigues de Sousa[6], Lily Rodriguez Bayona[142], Anand Roopsind[143], Agustín Rudas[137], Ervan Rutishauser[42,144], Kamariah Abu Salim[122], Rafael P. Salomão[145,146], Juliana Schietti[6], Douglas Sheil[147], Richarlly C. Silva[57,148], Javier Silva Espejo[149], Camila Silva Valeria[38], Marcos Silveira[57], Murielle Simo-Droissart[17], Marcelo Fragomeni Simon[70], James Singh[150], Yahn Carlos Soto Shareva[15], Clement Stahl[54], Juliana Stropp[151], Rahayu Sukri[122], Terry Sunderland[152,153], Martin Svátek[154], Michael D. Swaine[155], Varun Swamy[156], Hermann Taedoumg[17], Joey Talbot[1], James Taplin[157], David Taylor[158], Hans ter Steege[159,160], John Terborgh[25], Raquel Thomas[143], Sean C. Thomas[161], Armando Torres-Lezama[162], Peter Umunay[163,164], Luis Valenzuela Gamarra[15], Geertje van der Heijden[165], Peter van der Hout[166], Peter van der Meer[167], Mark van Nieuwstadt[168], Hans Verbeeck[99], Ronald Vernimmen[169], Alberto Vicentini[6], Ima Célia Guimarães Vieira[146], Emilio Vilanova Torre[170], Jason Vleminckx[36], Vincent Vos[172], Ophelia Wang[173], Lee J. T. White[124,174,175], Simon Willcock[176], John T. Woods[177], Verginia Wortel[178], Kenneth Young[179], Roderick Zagt[180], Lise Zemagho[17], Pieter A. Zuidema[50], Joeri A. Zwerts[178,181], Oliver L. Phillips[1]

Affiliations:

1       School of Geography, University of Leeds, Leeds, UK

2       Department of Natural Sciences, Manchester Metropolitan University, Manchester, UK

3       Department of Geography, University College London, London, UK

4       Mensuration Unit, Forestry Commission of Ghana, Kumasi, Ghana

5       Embrapa Roraima, Brazilian Agricultural Research Corporation (EMBRAPA), Brasília, Brazil

6       Instituto Nacional de Pesquisas da Amazônia (INPA), Manaus, Brazil

7       Department of Ecosystem Science and Sustainability, Colorado State University, USA

8       Department of Environment and Geography, University of York, York, UK

9       DR Congo Programme, Wildlife Conservation Society, Kisangani, Democratic Republic of Congo

10      Centre de Formation et de Recherche en Conservation Forestiere (CEFRECOF), Epulu, Democratic Republic of Congo

11      Faculté de Gestion de Ressources Naturelles Renouvelables, Université de Kisangani, Kisangani, Democratic Republic of Congo

12      Service of Wood Biology, Royal Museum for Central Africa, Tervuren, Belgium

13      Department of Environment, Laboratory of Wood Technology (Woodlab), Ghent University, Ghent, Belgium

14      Faculdade de Ciências Agrárias, Biológicas e Sociais Aplicadas, Universidade do Estado de Mato Grosso, Nova Xavantina-MT, Brazil

15      Jardín Botánico de Missouri, Oxapampa, Peru

16      School of Life Sciences, University of Lincoln, Lincoln, UK

17      Plant Systematics and Ecology Laboratory, Higher Teachers' Training College, University of Yaoundé I, Yaoundé, Cameroon

18      Geography, College of Life and Environmental Sciences, University of Exeter, Exeter, UK

19      Environmental Change Institute, School of Geography and the Environment, University of Oxford, Oxford, UK

20      Graduate School of Science and Engineering, Kagoshima University, Japan

21      School of Anthropology and Conservation, University of Kent, Canterbury, UK

22      Instituto de Biodiversidade e Florestas, Universidade Federal do Oeste do Pará, Santarém - PA, Brazil

23      Universidade do Estado de Mato Grosso, Cáceres - MT, Brazil

24      Escuela de Ciencias Agrícolas, Pecuarias y del Medio Ambiente, National Open University and Distance, Colombia

25      Center for Tropical Conservation, Nicholas School of the Environment, Duke University, Durham, NC, USA

26      Projeto Dinâmica Biológica de Fragmentos Florestais, Instituto Nacional de Pesquisas da Amazônia, Manaus, Brazil

27      Universidade Estadual de Campinas, Campinas - SP, Brazil

28      National Institute for Space Research (INPE), São José dos Campos-SP, Brazil

29      Museo de Historia Natural Noel Kempff Mercado, Universidad Autónoma Gabriel René Moreno, Santa Cruz, Bolivia

30      Wageningen Environmental Research, Wageningen, The Netherlands

31      Dirección de la Carrera de Biología, Universidad Autónoma Gabriel René Moreno, Santa Cruz, Bolivia

32      Department of Organismic and Evolutionary Biology, Harvard University, Cambridge, MA, USA

33      Programa de Ciencias del Agro y el Mar, Herbario Universitario, Barinas, Venezuela

34      Departamento de Biologia, Universidade Federal do Amazonas, Manaus, Brazil

35  Centre of Ecology and Hydrology, Penicuik, UK

36  International Center for Tropical Botany, Department of Biological Sciences, Florida International University, Florida, FL, USA

37  Centro de Energia Nuclear na Agricultura, Universidade de São Paulo, São Paulo, SP, Brazil

38  Lancaster Environment Centre, Lancaster University, Lancaster, UK

39  Centro Multidisciplinar, Universidade Federal do Acre, Cruzeiro do Sul - AC, Brazil

40  Institure of Integrative Biology, ETH Zurich, Zurich, Switzerland

41  Priestley International Centre for Climate, University of Leeds, Leeds, UK

42  Smithsonian Tropical Research Institute, Panama, Panama

43  Cary Institute of Ecosystem Studies, Millbrook, NY, USA

44  School of Geography, School of Geography, Leeds, UK

45  The Landscapes and Livelihoods Group, Edinburgh, UK

46  UR Forest& Societies, CIRAD, Montpellier, France

47  Isotope Bioscience Laboratory-ISOFYS, Ghent University, Gent, Belgium

48  Gembloux Agro-Bio Tech, University of Liège, Liège, Belgium

49  UMR Silva, INRA, Nancy, France

50  Department of Forest Ecology and Forest Management Group, Wageningen University, Wageningen, The Netherlands

51  CSIRO, Canberra, Australia

52  Congo Programme, Wildlife Conservation Society, Brazzavile, Republic of Congo

53  Woods Hole Research Center, Falmouth, MA, USA

54  Ecologie des Forêts de Guyane (ECOFOG), INRA, Kourou, French Guiana

55  Programa de Pós-Graduação Ecologia e Manejo de Recursos Naturais, Universidade Federal do Acre, Rio Branco - AC, Brazil

56  Herbario Alfredo Paredes, Universidad Central del Ecuador, Quito, Ecuador

57  Centro de Ciências Biológicas e da Natureza, Universidade Federal do Acre, Rio Branco - AC, Brazil

58  Laboratoire Évolution et Diversité Biologique - UMR 5174 (CNRS/IRD/UPS), CNRS, Toulouse, France

59  Rougier-Gabon, Libreville, Gabon

60  Nicholas School of the Environment, Duke University, Durham, NC, USA

61  Grantham Research Institute on Climate Change and the Environment, London, UK

62  Inventory & Monitoring Program, National Park Service, Fredericksburg, VA, USA

63  Smithsonian Institution, Washington, DC, USA

64  Proyecto Castaña, Made de Dios, Peru

65  Universidad Nacional de San Agustín de Arequipa, Arequipa, Peru

66  Instituto de Geociências, Faculdade de Meteorologia, Universidade Federal do Para, Belém - PA, Brazil

67  Faculty of Science, Department of Ecology and Environmental Sciences, Palacký University Olomouc, Olomouc, Czech Republic

68  Center for Tropical Forest Science, Smithsonian Tropical Research Institute, Panama, Panama

69  Facultad de Ciencias Biológicas, Universidad Nacional de la Amazonía Peruana, Iquitos, Peru

70  Embrapa Genetic Resources & Biotechnology, Brazilian Agricultural Research Corporation (EMBRAPA), Brasília, Brazil

71  Instituto de Investigaciones de la Amazonía Peruana, Iquitos, Peru

72  Ecologie des Forêts de Guyane (ECOFOG), CIRAD, Kourou, French Guiana

73      Department of Anthropology, The University of Texas at Austin, Austin, TX, USA

74      Forest Resources Management, Gembloux Agro-Bio Tech, University of Liège, Liège, Belgium

75      AMAP Lab, IRD, CIRAD, CNRS, INRA, Univ Montpellier, Montpellier, France

76      Socioecosistemas y Cambio Climatico, Fundacion con Vida, Medellín, Colombia

77      School of Forestry, Beijing Forestry University, Beijing, China

78      Institute of Biological Sciences, Universidade Federal do Pará, Belém - PA, Brazil

79      National Museum of Natural History, Smithsonian Institute, Washington, DC, USA

80      School of Geography, Earth and Environmental Sciences, University of Birmingham, Birmingham, UK

81      School of Geography, Earth and Environmental Sciences, University of Plymouth, Plymouth, UK

82      Embrapa Amazônia Oriental, Brazilian Agricultural Research Corporation (EMBRAPA), Brasília, Brazil

83      Universidad Nacional Jorge Basadre de Grohmann (UNJBG), Tacna, Peru

84      Forestry Research Institute of Ghana (FORIG), Kumasi, Ghana

85      Smithsonian Institution Forest Global Earth Observatory (ForestGEO), Smithsonian Tropical Research Institute, Washington, DC, USA

86      School of Biology, University of Leeds, Leeds, UK

87      128 Busbridge Lane, Godalming, Surrey, UK

88      Royal Botanic Garden Edinburgh, Edinburgh, UK

89      Lukuru Wildlife Research Foundation, Kinshasa, Democratic Republic of Congo

90      Division of Vertebrate Zoology, Yale Peabody Museum of Natural History, New Haven, CT, USA

91      Institute of Botany, Czech Academy of Sciences, Brno, Czech Republic

92      Department of Botany, Palacký University in Olomouc, Olomouc, Czech Republic

93      Instituto Venezolano de Investigaciones Científicas (IVIC), Caracas, Venezuela

94      Département Hommes, natures, sociétés, Muséum National d'Histoire Naturel, Paris, France

95      Universidad Nacional de San Antonio Abad del Cusco, Cusco, Peru

96      Biological and Environmental Sciences, University of Stirling, Stirling, UK

97      Instituto IMANI, Universidad Nacional de Colombia, Leticia, Colombia

98      Faculty of Science, Department of Botany and Plant Physiology, University of Buea, Buea, Cameroon

99      Department of Environment, Computational & Applied Vegetation Ecology (Cavelab), Ghent University, Ghent, Belgium

100     PELD, Universidade do Estado de Mato Grosso, Nova Xavantina-MT, Brazil

101     Tropical Peat Research Institute, Malaysian Palm Oil Board, Kuala Lumpur, Malaysia

102     Agteca, Santa Cruz, Bolivia

103     Graduate School of Agriculture, Kyoto University, Japan

104     Royal Botanic Gardens Kew, Richmond, London, UK

105     Department of Earth Sciences, University of Hong Kong, HKSAR

106     Centre for Tropical Environmental and Sustainability Science (TESS) and College of Marine and Environmental Sciences, James Cook University, Australia

107     Uganda Programme, Wildlife Conservation Society, Kampala, Uganda

108     Remote Sensing Division, National Institute for Space Research (INPE), São José dos Campos-SP, Brazil

109     Department of Ecology, University of Brasília, Brasília, Brazil

110     Environmental Science and Policy, George Mason University, Fairfax, VA, USA

[111] Botany Department, University of Ibadan, Ibadan, Nigeria

[112] Coordenação da Biodiversidade, Instituto Nacional de Pesquisas da Amazônia (INPA), Mauaus, Brazil

[113] cE3c – Centre for Ecology, Evolution and Environmental Changes / Azorean Biodiversity Group, Universidade dos Açores, Angra do Heroísmo, Azores, Portugal

[114] LIBRe – Laboratory for Integrative Biodiversity Research, Finnish Museum of Natural History, University of Helsinki, Helsinki, Finland

[115] Laboratório de Biogeoquímica Ambiental Wolfgang C. Pfeiffer, Universidade Federal de Rondônia, Porto Velho - RO, Brazil

[116] Faculdade de Ciências Agrárias, Biológicas e Sociais Aplicadas, Universidad do Estado de Mato Grosso, Nova Xavantina-MT, Brazil

[117] Tropical Forests and People Research Centre, University of the Sunshine Coast, Australia

[118] Flamingo Land Ltd., North Yorkshire, UK

[119] Centre for Ecology and Hydrology, Wallingford, UK

[120] School of International Tropical Forestry, Universiti Malaysia Sabah, Kota Kinabalu, Malaysia

[121] Escuela de Ciencias Forestales, Unidad Académica del Trópico, Universidad Mayor de San Simón, Sacta, Bolivia

[122] Faculty of Science, Universiti Brunei Darussalam, Brunei

[123] Agence Nationale des Parcs Nationaux, Libreville, Gabon

[124] Ministère de la Forêt, de la Mer, de l'Environnement, Chargé du Plan Climat, Libreville, Gabon

[125] University of Edinburgh, Edinburgh, UK

[126] Biologia Vegetal, Universide Estadual de Campinas, Campinas - SP, Brazil

[127] Facultad de Ingeniería Ambiental, Universidad Estatal Amazónica, Puyo, Pastaza, Ecuador

[128] Forest Research Centre, Sabah Forestry Department, Sepilok, Malaysia

[129] Carrera de Ingeniería Forestal, Universidad Tecnica del Norte, Ibarra, Ecuador

[130] Royal Botanical Garden Edinburgh, Edinburgh, UK

[131] Universidad Regional Amazónica IKIAM, Tena, Ecuador

[132] Public Communications and Outreach Group, Parks and Recreation Division, Oakland Park, FL, USA

[133] Keller Science Action Center, Field Museum, Chicago, IL, USA

[134] Centre for Agricultural Research in Suriname (CELOS), Paramaribo, Suriname

[135] Department of Forest Ecology and Forest Management Group, Wageningen University and Research, Wageningen, The Netherlands

[136] University of Oslo, Oslo, Norway

[137] Instituto de Ciencias Naturales, Universidad Nacional de Colombia, Leticia, Colombia

[138] Department of Biology, Boston University, Boston, USA

[139] Institute of Research for Forestry Development (INDEFOR), Universidad de los Andes, Mérida, Venezuela

[140] Bureau Waardenburg, Culemborg, The Netherlands

[141] Socioecosistemas y Cambio Climatico, Fundacion Con Vida, Medellín, Colombia

[142] Centro de Conservacion, Investigacion y Manejo de Areas Naturales, CIMA Cordillera Azul, Lima, Peru

[143] Iwokrama International Centre for Rainforest Conservation and Development, Georgetown, Guyana

[144] Carboforexpert, Geneva, Switzerland

[145] Universidade Federal Rural da Amazônia/CAPES, Belém - PA, Brazil

[146] Museu Paraense Emílio Goeldi, Belém - PA, Brazil

[147] Faculty of Environmental Sciences and Natural Resource Management, Norwegian University of Life Sciences, Ås, Norway

148    Instituto Federal do Acre, Rio Branco - AC, Brazil

149    Universidad de San Antonio Abad del Cusco, Cusco, Peru

150    Guyana Forestry Commission, Georgetown, Guyana

151    Federal University of Alagoas, Maceió, Brazil

152    Sustainable Landscapes and Food Systems, Center for International Forestry Research, Bogor, Indonesia

153    Faculty of Forestry, University of British Columbia, Vancouver, Canada

154    Department of Forest Botany, Dendrology and Geobiocoenology, Mendel University in Brno, Brno, Czech Republic

155    Department of Plant & Soil Science, School of Biological Sciences, University of Aberdeen, Aberdeen, UK

156    Institute for Conservation Research, San Diego Zoo, San Diego, USA

157    UK Research & Innovation, Innovate UK, London

158    Department of Geography, National University of Singapore, Singapore, Singapore

159    Naturalis Biodiversity Center, Leiden, The Netherlands

160    Systems Ecology, VU University, Amsterdam, The Netherlands

161    Faculty of Forestry, University of Toronto, Toronto, Canada

162    Universidad de los Andes, Merida, Colombia

163    Wildlife Conservation Society, New York, NY, USA

164    Yale School of Forestry & Environmental Studies, Yale University, New Haven, CT, USA

165    School of Geography, University of Notingham, Nottingham, UK

166    Van der Hout Forestry Consulting, Rotterdam, The Netherlands

167    Van Hall Larenstein University of Applied Sciences, Velp, The Netherlands

168    Utrecht University, Utrecht, The Netherlands

169    Deltares, Delft, The Netherlands

170    School of Environmental and Forest Sciences, University of Washington, Seattle, OR, USA

171    Department of Biological Sciences, Florida International University, Florida, FL, USA

172    Centro de Investigación y Promoción del Campesinado, La Paz, Bolivia

173    School of Earth Sciences and Environmental Sustainability, Northern Arizona University, Flagstaff, AZ, USA

174    Institut de Recherche en Ecologie Tropicale, Libreville, Gabon

175    School of Natural Sciences, University of Stirling, Stirling, UK

176    School of Natural Sciences, University of Bangor, Bangor, UK

177    University of Liberia, Monrovia, Liberia

178    Forest Management, Centre for Agricultural Research in Suriname (CELOS), Paramaribo, Suriname

179    Department of Geography and The Environment, University of Texas at Austin, Austin, TX, USA

180    Tropenbos International, Wageningen, The Netherlands

181    Biology, Utrecht University, Utrecht, The Netherlands

1    **Abstract**

2    The sensitivity of tropical forest carbon to climate is a key uncertainty in predicting global climate

3    change. While short-term drying and warming are known to impact forests it is unknown if such effects

4    translate into long-term responses. Here we analyse 590 permanent plots measured across the tropics to

5    derive the equilibrium climate controls on forest carbon. Maximum temperature is the most important

6    predictor of aboveground biomass (-9.1 Mg C ha$^{-1}$ $°C^{-1}$), primarily by reducing woody productivity, and

7    with a greater rate of decline in the hottest forests (>32.2 °C). Our results nevertheless reveal greater

8    thermal resilience than observations of short-term variation imply. To realise the long-term climate

9    adaptation potential of tropical forests requires both protecting them and stabilising the Earth's climate.

10

11    **One sentence summary.** Biome-wide variation in tropical forest carbon stocks and dynamics shows

12    long-term thermal resilience.

7

13    <u>Main text</u>

14    The response of tropical terrestrial carbon to environmental change is a critical component of global

15    climate models (*1*). Land-atmosphere feedbacks depend on the balance of positive biomass growth

16    stimulation by $CO_2$ fertilisation (i.e. β) and negative responses to warmer temperatures and any

17    change in precipitation (i.e. γ). Yet the climate response is so poorly constrained that it remains one of

18    the largest uncertainties in Earth system models (*2, 3*), with the temperature sensitivity of tropical land

19    carbon stocks alone differing by > 100 Pg C °C$^{-1}$ among models (*2*). Such uncertainty impedes our

20    understanding of the global carbon cycle, limiting our ability to simulate the future of the Earth

21    system under different long-term climate mitigation strategies. A critical long-term control on tropical

22    land-atmosphere feedbacks is the sensitivity to climate (γ) of tropical forests, where c. 40 % of the

23    world's vegetation carbon resides (*4*).

24    The sensitivity to environmental change of tropical biomass carbon stocks, their rate of production

25    and their persistence, can all be estimated by relating their short-term and inter-annual responses to

26    variation in climate (*5-7*). These sensitivities are then used to constrain longer-term projections of

27    climate responses (*2*). Such approaches typically find that higher minimum temperatures are strongly

28    associated with slower tree growth and reduced forest carbon stocks, likely due to increased

29    respiration at higher temperatures (*7-9*). Tropical forest carbon is also sensitive to precipitation (*10*),

30    with, for example, elevated tree mortality occurring during drought events (*11*).

31    Yet the sensitivity of ecosystems to inter-annual fluctuations may be an unreliable guide to their

32    longer-term responses to climate change. Such responses will also be influenced by physiological

33    acclimation (*12*), changes in demographic rates (*13*), and shifts in species composition (*14*). For

34    example, both respiration and photosynthesis can acclimate under sustained temperature increases

35    (*15-17*), and tropical trees exhibit physiological plasticity (*18*) and shifts in species composition (*14*)

36    under sustained drought. These processes could mean that tropical forests are less sensitive to climate

37    than estimates derived from inter-annual variability imply. An alternative, complimentary approach to

38    assessing sensitivity to climate is to measure and analyse spatial variation in tropical ecosystems

39    across climate gradients as a space-for-time substitution. Such biome-wide spatial variation in forest

8

40  carbon stocks, fluxes and persistence offers a unique and largely unexplored window into the potential

41  equilibrium sensitivity of tropical forest vegetation to warming, as it captures real-world vegetation

42  responses that allow for physiological and ecological adaptation (*12*).

43  To assess the long-term climate controls on tropical forest growth and carbon stocks, here we have

44  assembled, measured, and analysed a pan-tropical network of 590 permanent, long-term inventory

45  plots (Fig. 1, see Figs. S1-2 for ability to capture biome climate space). Our analysis combines

46  standardised measurements from across South American, African, Asian and Australian tropical

47  lowland forests (273, 239, 61 and 17 plots respectively). For every plot we calculated aboveground

48  carbon stocks (*19*). Then, to better assess the dynamic controls on aboveground carbon stocks, we

49  also computed the rate of carbon gained by the system (aboveground woody carbon production,

50  calculated as tree growth plus newly recruited trees, in Mg C ha$^{-1}$ yr$^{-1}$), and the carbon residence time

51  in living biomass (calculated as the ratio of living C stocks to C gains, in years).

52  We find considerable variation in biomass carbon among continents, with lower stocks per unit area

53  in South America compared with the Paleotropics even after accounting for environmental variables

54  (Fig. 1). Continents with high carbon stocks had either large carbon gains (Asia), or long carbon

55  residence times (Africa, Fig. 1). Because of these differences among continents, which are potentially

56  due to differences in evolutionary history (*20*), we analyse the environmental drivers of spatial

57  variation in carbon stocks while accounting for biogeographical differences. We fitted linear models

58  with explanatory variables representing hypothesised mechanistic controls of climate on tropical

59  forest carbon (Table S1). We also included soil covariates, continent intercepts and eigenvectors

60  describing spatial relationships amongst plots to account for other sources of variation (*21*).

61  Forest carbon stocks were most strongly related to maximum temperature (-5.9 % per 1°C increase in

62  maximum temperature, 95 % CI = -8.6 to -3.1 %, Fig. 2, equivalent to -9.1 Mg C ha$^{-1}$ °C$^{-1}$ for a stand

63  with the mean carbon stocks in our dataset, 154.6 Mg C ha$^{-1}$), followed by rainfall (+2.4 % per 100

64  mm increase in precipitation in the driest quarter, 95 % CI = 0.6 – 4.3 %, Fig. 2, equivalent to 0.04

65  Mg C ha$^{-1}$ mm$^{-1}$ for a stand with the mean carbon stocks in our dataset), with no statistically

66  significant relationship with minimum temperature, wind speed or cloud cover (Fig 2). The effects of

9

67 maximum temperature and precipitation are also evident in an analysis considering a wider suite of

68 climate variables than those tied to hypothesised mechanisms (Fig. S3), and in an additional

69 independent pantropical dataset of 223 single-census plots (for which carbon gains and residence time

70 cannot be assessed, Fig. S4).

71 The negative effect of maximum temperature on aboveground carbon stocks mainly reflects reduced

72 carbon gains with increasing temperature (-4.0 % per 1°C, 95% CI = -6.2 to -1.8 %, Fig. 2) while the

73 positive effect of precipitation emerges through longer carbon residence times with increasing

74 precipitation in the driest quarter (3.3 % per 100 mm, 95 % CI = 0.9 – 5.7 %, Fig. 2). Carbon

75 residence time also increased with the proportion of clay in the soil (Fig. 2). The additive effects of

76 precipitation and temperature on carbon stocks were modified by an interaction between them ($\Delta$ AIC

77 = 15.4 comparing full linear model with or without interaction), with temperature effects more

78 negative when precipitation is low (Fig. S6). The interaction was through shortening carbon residence

79 time ($\Delta$ AIC = 11.9) rather than reducing carbon gains (model without interaction better, $\Delta$ AIC =

80 1.4).

81 An alternative analysis using decision tree algorithms (22) also showed maximum temperature and

82 precipitation to be important (Fig. S7). This decision tree approach, which can capture complex non-

83 linear relationships (22), indicated potential non-linearity in the relationships between carbon stocks

84 and both temperature and precipitation, with the positive effect of increasing dry season precipitation

85 on residence times strengthening when precipitation was low, and the negative effect of maximum

86 temperature intensifying at high temperatures (Fig. S7).

87 We further investigated non-linearity in the temperature relationship using breakpoint regression

88 (supported over linear regression based on lower AIC, $\Delta$ AIC = 15.0), which revealed that above 32.2

89 °C (95 % CI = 31.7 – 32.6 °C) the relationship between carbon stocks and maximum temperature

90 became more negative (cooler than breakpoint: -3.8 % °C$^{-1}$, warmer than breakpoint: -14.7 % °C$^{-1}$,

91 Fig. 3). By partitioning carbon stocks into their production and persistence we find that this non-

92 linearity reflects changes to carbon residence time ($\Delta$ AIC = 10.6) rather than gains ($\Delta$ AIC = 1.7).

93 Overall, our results thus indicate two separate climate controls on carbon stocks: a negative linear

10

94      effect of maximum temperature through reduced carbon gains, and a non-linear negative effect of

95      maximum temperature, ameliorated by high dry-season precipitation, through reduced carbon

96      residence time.

97      The effect of temperature on carbon residence time only emerges when dry season precipitation is low

98      so is consistent with theoretical expectations that negative effects of temperature on tree longevity are

99      exacerbated by moisture limitation, rather than being independent of it and due to increased

100     respiration costs alone (*23*). This could occur through high vapour pressure deficits in hot and dry

101     forests increasing mortality risk by causing hydraulic stress (*23, 24*), or carbon starvation due to

102     limited photosynthesis as a result of stomatal closure (*23*). Notably, the temperature-precipitation

103     interaction we find for aboveground stocks is in the opposite direction to temperature-precipitation

104     interactions reported for soil carbon. In soils, moisture limitation suppresses the temperature response

105     of heterotrophic respiration (*25*), while in trees moisture limitation enhances the mortality risks of

106     high temperatures.

107     The temperature effects on biomass carbon stocks and gains are primarily due to maximum rather

108     than minimum temperature. This is consistent with high daytime temperatures reducing $CO_2$

109     assimilation rates, for example due to increased photorespiration or longer duration of stomatal

110     closure (*26, 27*), whereas if negative temperature effects were to have increased respiration rates there

111     should be a stronger relationship with minimum (i.e. night-time) temperature. Critically, minimum

112     temperature is unrelated to aboveground carbon stocks both pan-tropically and in the one continent,

113     South America, where maximum and minimum temperature are largely decoupled ($r = 0.33$; Fig. S8).

114     While carbon gains are negatively related to minimum temperature (Fig S9) this bivariate relationship

115     is weaker than with maximum temperature, and disappears once the effects of other variables are

116     accounted for (Fig. 2). Finally, in Asia, the tropical region which experiences the warmest minimum

117     temperatures of all, both carbon stocks and carbon gains are highest (Fig. 1, Fig. S11).

118     Overall our results suggest that tropical forests have considerable potential to acclimate and adapt to

119     the effects of night-time minimum temperatures, but are clearly sensitive to the effects of daytime

120     maximum temperature. This is consistent with ecophysiological observations suggesting that the

121  acclimation potential of respiration (*15*) is greater than that of photosynthesis (*17*). The temperature

122  sensitivity revealed by our analysis is also considerably weaker than short-term sensitivities

123  associated with inter-annual climate variation (*8*). For example, by relating short-term annual climate

124  anomalies to responses in plots, the effect of a 1°C increase in temperature on carbon gains has been

125  estimated as more than three-fold our long-term, pantropical result (*28*). This stronger long-term

126  thermal resilience is likely due to a combination of individual acclimation and plasticity (*15-17*),

127  differences in species' climate responses (*29*) leading to shifts in community composition due to

128  changing demographic rates (*12*) and the immigration of species with higher performance at high

129  temperatures (*12*).

130  Our pantropical analysis of the sensitivity to climate of aboveground forest carbon stocks, gains and

131  persistence shows that warming reduces carbon stocks and gains from woody productivity. Using a

132  reference carbon stock map (*30*) and applying our estimated temperature sensitivity (including non-

133  linearity) while holding other variables constant leads to an eventual biome-wide reduction of 14.1 Pg

134  C in live biomass (including scaling to estimate carbon in roots) for a 1°C increase in maximum

135  temperature (95 % CI = 6.9 – 20.7 Pg). This compares with a large range of projected sensitivities in

136  the subset of coupled climate carbon cycle models that report vegetation carbon (1 – 58 Pg C °C$^{-1}$),

137  although we note that these models have not been run to equilibrium (see SI Methods).

138  Our results suggest that stabilising global surface temperatures at 2°C above pre-industrial levels will

139  cause a potential long-term biome-wide loss of 35.3 Pg C (95 % CI = 20.9 – 49.0 Pg, estimates with

140  alternative baseline biomass maps 24.0 – 28.4 Pg, Fig. S12). The greatest long-term reductions in

141  carbon stocks are projected in South America, where baseline temperatures and future warming are

142  both highest (Fig. 4, Fig. S13). This warming would push 71 % of the biome beyond the thermal

143  threshold – maximum temperature of 32.2°C – where larger long-term reductions in biomass are

144  expected (Fig. S14). Of course, growth stimulation by carbon dioxide (*31*) will partially or wholly

145  offset the effect of this temperature increase, depending on both the level of atmospheric carbon

146  dioxide that limits warming to 2°C above pre-industrial levels and the fertilization effect of this

147  carbon dioxide on tropical trees. Although $CO_2$ fertilisation is expected to reduce temperature induced

148    carbon losses from biomass across the tropics (Table S3), our analysis indicates that $CO_2$ fertilisation

149    is not enough to offset long-term temperature induced carbon losses within Amazonia (Fig. S15).

150    The long-term climate sensitivities derived from our pan-tropical field measurements incorporate

151    ecophysiological and ecological adaptation, and so provide an estimate of the long-term, quasi-

152    equilibrium, response of tropical vegetation to climate. We note that this thermal adaptation potential

153    may not be fully realised in future responses because (i) the speed of temperature rises may exceed

154    species' adaptive capabilities, (ii) habitat fragmentation may limit species' ability to track changes in

155    the environment, and (iii) other human impacts such as logging and fire can increase the vulnerability

156    of forest carbon stocks to high temperatures. While many tropical forests are under severe threat of

157    conversion, our results show that, in the long-run, tropical forests that remain intact can continue to

158    store high levels of carbon under high temperatures. Achieving the biome-wide climate resilience

159    potential we document depends on limiting heating and on large-scale conservation and restoration to

160    protect biodiversity and allow species to move.

161

162

**163    References and Notes**

164    1.    P. M. Cox, R. A. Betts, C. D. Jones, S. A. Spall, I. J. Totterdell, Acceleration of global
165         warming due to carbon-cycle feedbacks in a coupled climate model. *Nature* **408**, 184 (2000).
166    2.    P. M. Cox *et al.*, Sensitivity of tropical carbon to climate change constrained by carbon
167         dioxide variability. *Nature* **494**, 341-344 (2013).
168    3.    B. B. B. Booth *et al.*, High sensitivity of future global warming to land carbon cycle
169         processes. *Environmental Research Letters* **7**, 024002 (2012).
170    4.    K.-H. Erb *et al.*, Unexpectedly large impact of forest management and grazing on global
171         vegetation biomass. *Nature* **553**, 73 (2017).
172    5.    W. Wang *et al.*, Variations in atmospheric $CO_2$ growth rates coupled
173         with tropical temperature. *Proceedings of the National Academy of Sciences* **110**, 13061
174         (2013).
175    6.    J. Liu *et al.*, Contrasting carbon cycle responses of the tropical continents to the 2015–2016
176         El Niño. *Science* **358**, eaam5690 (2017).
177    7.    D. A. Clark, S. C. Piper, C. D. Keeling, D. B. Clark, Tropical rain forest tree growth and
178         atmospheric carbon dynamics linked to interannual temperature variation during 1984–2000.
179         *Proceedings of the National Academy of Sciences* **100**, 5852 (2003).
180    8.    W. R. L. Anderegg *et al.*, Tropical nighttime warming as a dominant driver of variability in
181         the terrestrial carbon sink. *Proceedings of the National Academy of Sciences* **112**, 15591-
182         15596 (2015).
183    9.    A. Ballantyne *et al.*, Accelerating net terrestrial carbon uptake during the warming hiatus due
184         to reduced respiration. *Nature Climate Change* **7**, 148 (2017).
185    10.   J. K. Green *et al.*, Large influence of soil moisture on long-term terrestrial carbon uptake.
186         *Nature* **565**, 476-479 (2019).
187    11.   O. L. Phillips *et al.*, Drought Sensitivity of the Amazon Rainforest. *Science* **323**, 1344 (2009).
188    12.   M. D. Smith, A. K. Knapp, S. L. Collins, A framework for assessing ecosystem dynamics in
189         response to chronic resource alterations induced by global change. *Ecology* **90**, 3279-3289
190         (2009).
191    13.   J. H. Brown, T. J. Valone, C. G. Curtin, Reorganization of an arid ecosystem in response to
192         recent climate change. *Proceedings of the National Academy of Sciences* **94**, 9729-9733
193         (1997).
194    14.   S. Fauset *et al.*, Drought-induced shifts in the floristic and functional composition of tropical
195         forests in Ghana. *Ecol Lett* **15**, 1120-1129 (2012).
196    15.   A. Gunderson Carla, H. O'Hara Keiran, M. Campion Christina, V. Walker Ashley, T.
197         Edwards Nelson, Thermal plasticity of photosynthesis: the role of acclimation in forest
198         responses to a warming climate. *Global Change Biology* **16**, 2272-2286 (2010).
199    16.   M. Slot *et al.*, Thermal acclimation of leaf respiration of tropical trees and lianas: response to
200         experimental canopy warming, and consequences for tropical forest carbon balance. *Global
201         Change Biology* **20**, 2915-2926 (2014).
202    17.   F. Ow Lai, L. Griffin Kevin, D. Whitehead, S. Walcroft Adrian, H. Turnbull Matthew,
203         Thermal acclimation of leaf respiration but not photosynthesis in Populus deltoides×nigra.
204         *New Phytologist* **178**, 123-134 (2008).
205    18.   T. F. Domingues *et al.*, Ecophysiological plasticity of Amazonian trees to long-term drought.
206         *Oecologia* **187**, 933-940 (2018).
207    19.   See supplimentary material.
208    20.   J. W. F. Slik *et al.*, Phylogenetic classification of the world's tropical forests. *Proceedings of
209         the National Academy of Sciences* **115**, 1837 (2018).
210    21.   S. Dray, P. Legendre, P. R. Peres-Neto, Spatial modelling: a comprehensive framework for
211         principal coordinate analysis of neighbour matrices (PCNM). *Ecological Modelling* **196**, 483-
212         493 (2006).
213    22.   L. Breiman, Random Forests. *Machine Learning* **45**, 5-32 (2001).
214    23.   N. McDowell *et al.*, Drivers and mechanisms of tree mortality in moist tropical forests. *New
215         Phytologist* **219**, 851-869 (2018).

14

216 24.     G. Fontes Clarissa *et al.*, Dry and hot: the hydraulic consequences of a climate change–type
217       drought for Amazonian trees. *Philosophical Transactions of the Royal Society B: Biological*
218       *Sciences* **373**, 20180209 (2018).
219 25.     P. Ciais *et al.*, Europe-wide reduction in primary productivity caused by the heat and drought
220       in 2003. *Nature* **437**, 529-533 (2005).
221 26.     M. E. Dusenge, A. G. Duarte, D. A. Way, Plant carbon metabolism and climate change:
222       elevated CO2 and temperature impacts on photosynthesis, photorespiration and respiration.
223       *New Phytologist* **221**, 32-49 (2019).
224 27.     S. Pau, M. Detto, Y. Kim, C. J. Still, Tropical forest temperature thresholds for gross primary
225       productivity. *Ecosphere* **9**, e02311 (2018).
226 28.     D. A. Clark, D. B. Clark, S. F. Oberbauer, Field-quantified responses of tropical rainforest
227       aboveground productivity to increasing CO2 and climatic stress, 1997-2009. *J. Geophys.*
228       *Res.-Biogeosci.* **118**, 783-794 (2013).
229 29.     W. R. L. Anderegg *et al.*, Hydraulic diversity of forests regulates ecosystem resilience during
230       drought. *Nature* **561**, 538-541 (2018).
231 30.     V. Avitabile *et al.*, An integrated pan-tropical biomass map using multiple reference datasets.
232       *Global Change Biology* **22**, 1406-1420 (2016).
233 31.     S. Piao *et al.*, Evaluation of terrestrial carbon cycle models for their response to climate
234       variability and to CO2 trends. *Global Change Biology* **19**, 2117-2132 (2013).
235
236 References in SI only:
237 32.     A. B. Anderson, White-sand vegetation of Brazilian Amazonia. *Biotropica* **13**, 199-210
238       (1981).
239 33.     S. R. Pezeshki, Root responses of flood-tolerant and flood-sensitive tree species to soil redox
240       conditions. *Trees* **5**, 180-186 (1991).
241 34.     O. L. Phillips, T. R. Baker, T. R. Feldpausch, R. J. W. Brienen, "RAINFOR Field Manual for
242       Plot Establishment and Remeasurement," (2001).
243 35.     J. Talbot *et al.*, Methods to estimate aboveground wood productivity from long-term forest
244       inventory plots. *Forest Ecology and Management* **320**, 30-38 (2014).
245 36.     D. B. Clark, D. A. Clark, Landscape-scale variation in forest structure and biomass in a
246       tropical rain forest. *Forest ecology and management* **137**, 185-198 (2000).
247 37.     G. Lopez-Gonzalez, S. L. Lewis, M. Burkitt, O. L. Phillips, ForestPlots.net: a web application
248       and research tool to manage and analyse tropical forest plot data. *Journal of Vegetation*
249       *Science* **22**, 610-613 (2011).
250 38.     G. Lopez-Gonzalez, S. L. Lewis, M. Burkitt, T. R. Baker, O. L. Phillips.
251       (www.forestplots.net, 2009).
252 39.     R. J. W. Brienen *et al.*, Long-term decline of the Amazon carbon sink. *Nature* **519**, 344-348
253       (2015).
254 40.     J. Chave *et al.*, Improved allometric models to estimate the aboveground biomass of tropical
255       trees. *Global Change Biology* **20**, 3177-3190 (2014).
256 41.     J. Chave *et al.*, Towards a worldwide wood economics spectrum. *Ecology Letters* **12**, 351-366
257       (2009).
258 42.     A. E. Zanne *et al.* (Dryad Data Repository, 2009).
259 43.     R. C. Goodman *et al.*, Amazon palm biomass and allometry. *Forest Ecology and*
260       *Management* **310**, 994-1004 (2013).
261 44.     M. J. P. Sullivan *et al.*, Field methods for sampling tree height for tropical forest biomass
262       estimation. *Methods in Ecology and Evolution* **9**, 1179-1189 (2018).
263 45.     S. C. Thomas, Asymptotic height as a predictor of growth and allometric characteristics in
264       malaysian rain forest trees. *American Journal of Botany* **83**, 556-566 (1996).
265 46.     T. R. Feldpausch *et al.*, Tree height integrated into pantropical forest biomass estimates.
266       *Biogeosciences* **9**, 3381-3403 (2012).
267 47.     T. S. Kohyama, T. I. Kohyama, D. Sheil, Definition and estimation of vital rates from
268       repeated censuses: Choices, comparisons and bias corrections focusing on trees. *Methods in*
269       *Ecology and Evolution* **9**, 809-821 (2018).

48. A. R. Martin, M. Doraisami, S. C. Thomas, Global patterns in wood carbon concentration across the world's trees and forests. *Nature Geoscience* **11**, 915-920 (2018).

49. D. Galbraith *et al.*, Residence times of woody biomass in tropical forests. *Plant Ecology & Diversity* **6**, 139-157 (2013).

50. G. Lopez-Gonzalez, M. J. P. Sullivan, T. R. Baker. (2015).

51. S. E. Fick, R. J. Hijmans, WorldClim 2: new 1-km spatial resolution climate surfaces for global land areas. *International Journal of Climatology* **37**, 4302-4315 (2017).

52. R. J. Hijmans, S. Phillips, J. Leathwick, J. Elith, dismo: Species distribution modeling. R package version 1.0-12. *The R Foundation for Statistical Computing, Vienna http://cran. r-project. org*, (2015).

53. A. M. Wilson, W. Jetz, Remotely Sensed High-Resolution Global Cloud Dynamics for Predicting Ecosystem and Biodiversity Distributions. *PLOS Biology* **14**, e1002415 (2016).

54. M. New, D. Lister, M. Hulme, I. Makin, A high-resolution data set of surface climate over global land areas. *Climate research* **21**, 1-25 (2002).

55. T. Hengl *et al.*, SoilGrids250m: Global gridded soil information based on machine learning. *PLOS ONE* **12**, e0169748 (2017).

56. P. R. Peres-Neto, P. Legendre, Estimating and controlling for spatial structure in the study of ecological communities. *Global Ecology and Biogeography* **19**, 174-184 (2010).

57. S. L. Lewis *et al.*, Increasing carbon storage in intact African tropical forests. *Nature* **457**, 1003 (2009).

58. K. Barton, 2015.

59. V. M. R. Muggeo, Estimating regression models with unknown break-points. *Statistics in Medicine* **22**, 3055-3071 (2003).

60. A. Liaw, M. Wiener, Classificiation and Regression by randomForest. *R News* **2**, 18-22 (2002).

61. D. M. Olson *et al.*, Terrestrial Ecoregions of the World: A New Map of Life on EarthA new global map of terrestrial ecoregions provides an innovative tool for conserving biodiversity. *BioScience* **51**, 933-938 (2001).

62. M. C. Hansen *et al.*, High-Resolution Global Maps of 21st-Century Forest Cover Change. *Science* **342**, 850-853 (2013).

63. R. Jackson *et al.*, A global analysis of root distributions for terrestrial biomes. *Oecologia* **108**, 389-411 (1996).

64. S. S. Saatchi *et al.*, Benchmark map of forest carbon stocks in tropical regions across three continents. *Proceedings of the National Academy of Sciences* **108**, 9899-9904 (2011).

65. A. Baccini *et al.*, Estimated carbon dioxide emissions from tropical deforestation improved by carbon-density maps. *Nature Climate Change* **2**, 182-185 (2012).

66. E. T. A. Mitchard *et al.*, Uncertainty in the spatial distribution of tropical forest biomass: a comparison of pan-tropical maps. *Carbon Balance and Management* **8**, 10 (2013).

67. E. T. Mitchard *et al.*, Markedly divergent estimates of A mazon forest carbon density from ground plots and satellites. *Global Ecology and Biogeography* **23**, 935-946 (2014).

68. R. J. Hijmans. (2005). WorldClim - Global Climate Data. www.worldclim.org.

69. R. J. Hijmans, S. E. Cameron, J. L. Parra, P. G. Jones, A. Jarvis, Very high resolution interpolated climate surfaces for global land areas. *International Journal of Climatology* **25**, 1965-1978 (2005).

70. B. Kirtman *et al.*, Near-term climate change: projections and predictability. (2013).

71. H. D. Matthews, K. Caldeira, Stabilizing climate requires near-zero emissions. *Geophysical Research Letters* **35**, (2008).

72. M. Meinshausen *et al.*, The RCP greenhouse gas concentrations and their extensions from 1765 to 2300. *Climatic Change* **109**, 213 (2011).

73. W. Kolby Smith *et al.*, Large divergence of satellite and Earth system model estimates of global terrestrial CO2 fertilization. *Nature Climate Change* **6**, 306 (2015).

74. D. W. Kicklighter *et al.*, A first-order analysis of the potential role of CO2 fertilization to affect the global carbon budget: a comparison of four terrestrial biosphere models. *Tellus B: Chemical and Physical Meteorology* **51**, 343-366 (1999).

16

324 75. Y. Malhi *et al.*, The linkages between photosynthesis, productivity, growth and biomass in
325 lowland Amazonian forests. *Global Change Biology* **21**, 2283-2295 (2015).
326 76. C. Terrer *et al.*, Nitrogen and phosphorus constrain the CO2 fertilization of global plant
327 biomass. *Nature Climate Change* **9**, 684-689 (2019).
328 77. S. Wenzel, P. M. Cox, V. Eyring, P. Friedlingstein, Emergent constraints on climate-carbon
329 cycle feedbacks in the CMIP5 Earth system models. *Journal of Geophysical Research:*
330 *Biogeosciences* **119**, 794-807 (2014).
331 78. K. E. Taylor, R. J. Stouffer, G. A. Meehl, An overview of CMIP5 and the experiment design.
332 *Bulletin of the American Meteorological Society* **93**, 485-498 (2012).
333 79. The CMIP5 model data is available via the Earth System Grid Federation.
334 80. E. Bartholome, A. S. Belward, GLC2000: a new approach to global land cover mapping from
335 Earth observation data. *International Journal of Remote Sensing* **26**, 1959-1977 (2005).
336 81. J. Chave *et al.*, Tree allometry and improved estimation of carbon stocks and balance in
337 tropical forests. *Oecologia* **145**, 87-99 (2005).
338 82. M. Slot, K. Winter, In situ temperature response of photosynthesis of 42 tree and liana species
339 in the canopy of two Panamanian lowland tropical forests with contrasting rainfall regimes.
340 *New Phytologist* **214**, 1103-1117 (2017).
341 83. Y. Malhi, The productivity, metabolism and carbon cycle of tropical forest vegetation.
342 *Journal of Ecology* **100**, 65-75 (2012).
343 84. E. A. Graham, S. S. Mulkey, K. Kitajima, N. G. Phillips, S. J. Wright, Cloud cover limits net
344 CO2 uptake and growth of a rainforest tree during tropical rainy seasons. *Proceedings of the*
345 *National Academy of Sciences* **100**, 572-576 (2003).
346 85. W. F. Laurance, T. J. Curran, Impacts of wind disturbance on fragmented tropical forests: A
347 review and synthesis. *Austral Ecology* **33**, 399-408 (2008).

348

349

412 **Supplementary Materials:**

413 Materials and Methods

414 Figures S1-S15

415 Tables S1-S3

416 References (32-85)

417
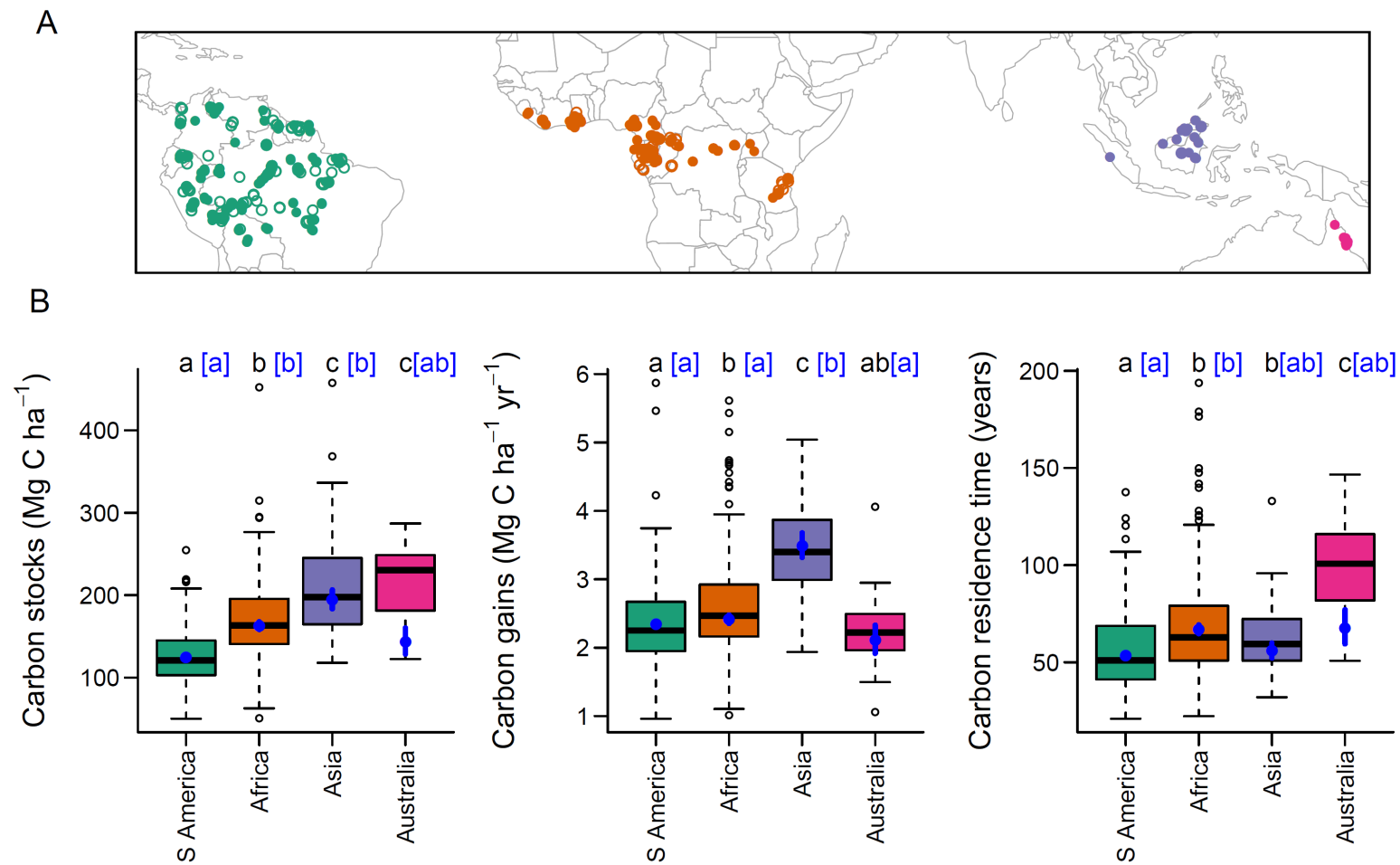


**Figure 1.** Spatial variation in tropical forest carbon. (A) Our plot network. Filled symbols show multi-census plots used in the main analysis, open symbols show single-census plots used as an independent dataset. (B) Variation in carbon among continents. Boxplots show raw variation while blue points show estimated mean values (± SE) after accounting for environmental variation. Letters denote statistically significant differences between continents (P < 0.05) based on raw data (black) or accounting for environmental effects (blue, square brackets).

423

424

425

426



427
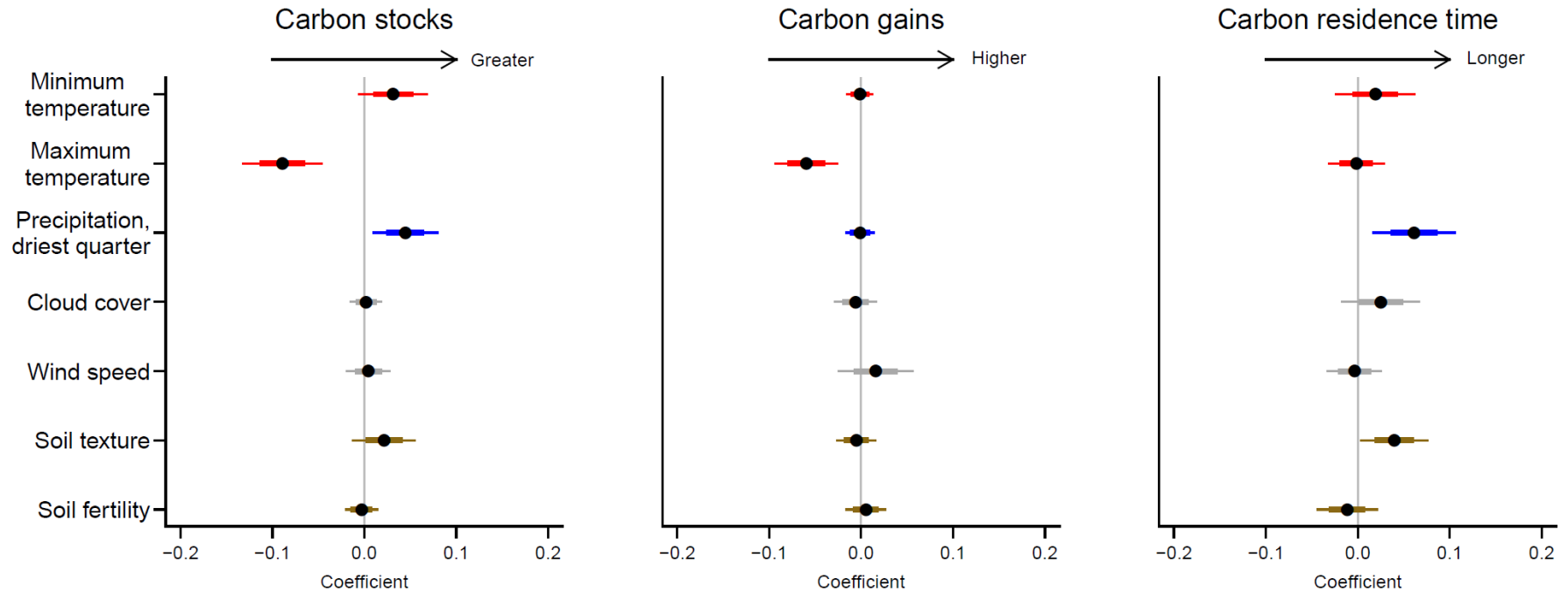
**Figure 2.** Correlates of spatial variation in tropical forest carbon. Points show coefficients from model-averaged general linear models. Variables that did not occur in well-supported models are shrinkage adjusted towards zero. Coefficients are standardised so that they represent change in the response variable for one standard deviation change in the explanatory variable. Error bars show standard errors (thick lines) and 95% confidence intervals (thin lines). Soil texture is represented by the percentage clay, and soil fertility by cation exchange capacity. The full models explained 44.1 %, 31.4 % and 30.9 % of spatial variation in carbon stocks, gains and residence time respectively. Coefficients are shown in Table S2. Results are robust to using an alternative allometry to estimate tree biomass (Fig. S5).

434
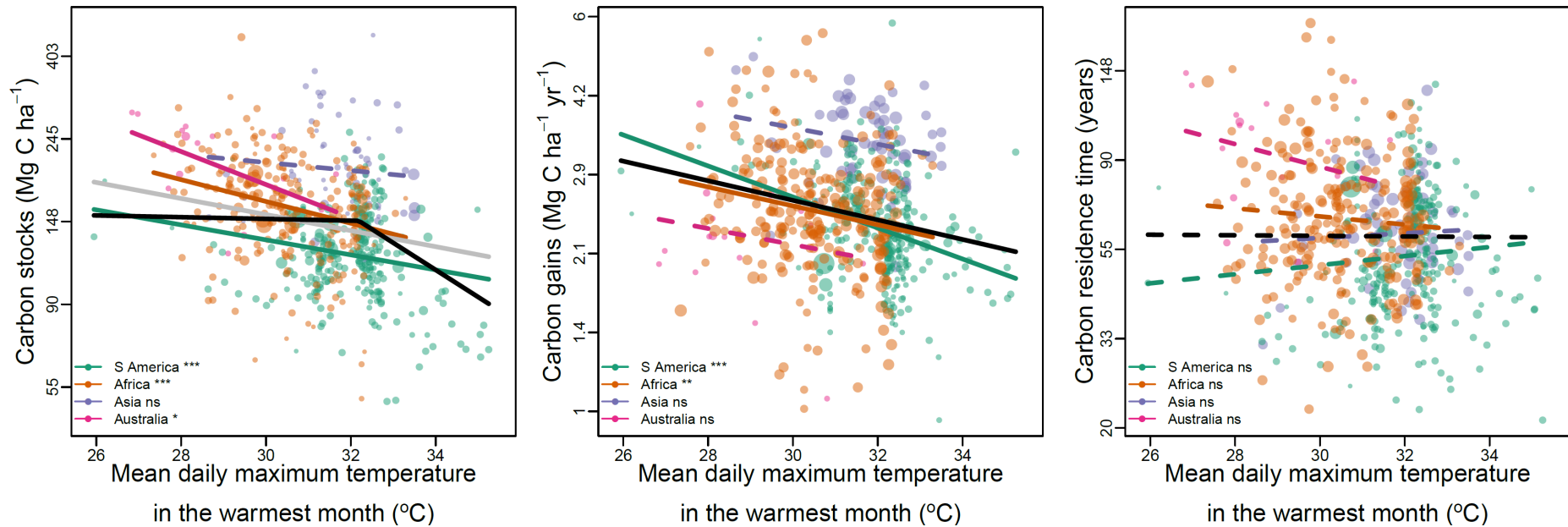
**Figure 3.** Temperature effects on tropical forest carbon stocks, carbon gains from woody productivity and carbon residence time. Black lines show the best pan-tropical relationships accounting for environmental covariates. The grey line shows the additional linear pan-tropical relationship for carbon stocks. Coloured lines show bivariate relationships within each continent. Statistically significant relationships are shown with solid lines, non-significant with dashed lines. Note that the y-axis is on a log-scale. Symbol point size is proportional to weights used in model fitting based on plot size and monitoring length, see SI Materials and Methods. For stocks and gains linear and break-point pan-tropical relationships are all statistically significant ($P < 0.001$), as are better sampled continents. For carbon residence time, relationships with temperature are non-significant but there is a statistically significant interaction between maximum temperature and precipitation in the driest quarter (Figure S6). Relationships with other variables are shown in Fig. S8-S10. *** $P < 0.001$, ** $P < 0.01$, * $P < 0.05$, ns $P \geq 0.05$

23

445

Δ Carbon stocks (Mg ha$^{-1}$)

Δ Carbon stocks (%)

446
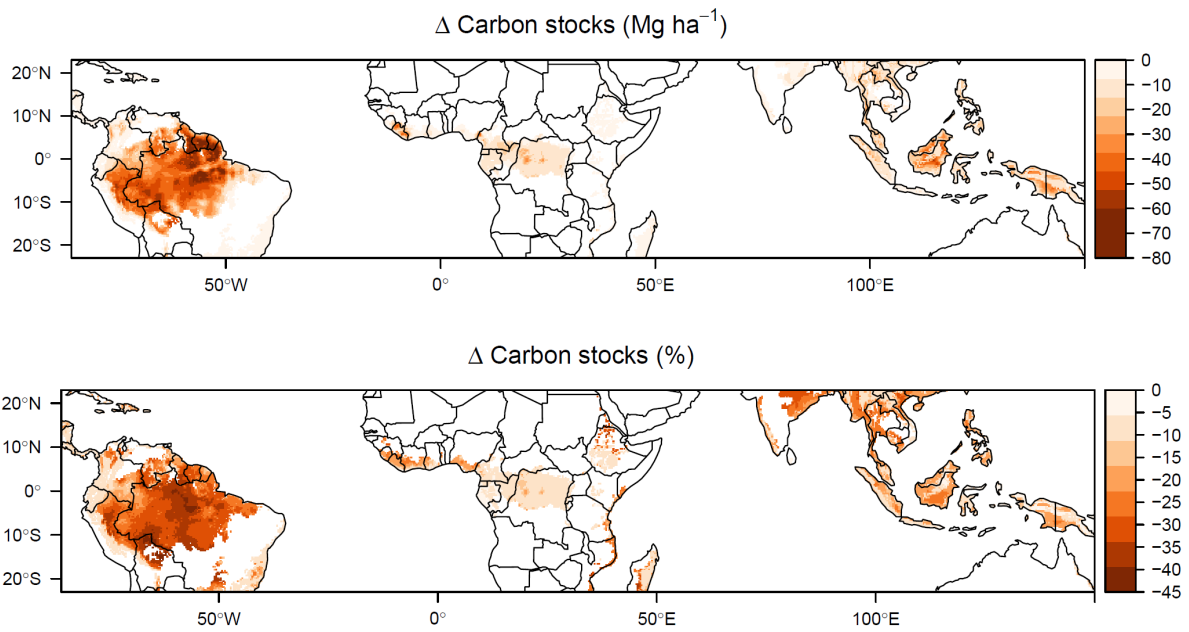
**Figure 4.** Long-term change in carbon stocks due to global surface temperature warming of approximately 2°C. Maps show the predicted absolute and relative change in tropical forest carbon stocks. Note that parts of the biome become warmer than currently observed in our dataset (Fig. S14). See Fig. S12 for predictions using alternative carbon reference maps. Predictions are based on temperature alone and do not include precipitation changes (for which future patterns of change are uncertain) or potential moderation via elevated $CO_2$ (see Fig. S15 for analysis incorporating this).

453

454

455 **Supporting information for Long-term thermal Sensitivity of the Earth's Tropical**

456 **Forests**

457 Martin J. P. Sullivan[1,2], Simon L. Lewis[1,3], Kofi Affum-Baffoe[4], Carolina Castilho[5], Flávia Costa[6], Aida
458 Cuni Sanchez[7,8], Corneille E. N. Ewango[9,10,11], Wannes Hubau[1,12,13], Beatriz Marimon[14], Abel Monteagudo-
459 Mendoza[15], Lan Qie[16], Bonaventure Sonké[17], Rodolfo Vasquez Martinez[15], Timothy R Baker[1], Roel J. W.
460 Brienen[1], Ted R. Feldpausch[18], David Galbraith[1], Manuel Gloor[1], Yadvinder Malhi[19], Shin-Ichiro Aiba[20],
461 Miguel N. Alexiades[21], Everton C. Almeida[22], Edmar Almeida de Oliveira[23], Esteban Álvarez Dávila[24],
462 Patricia Alvarez Loayza[25], Ana Andrade[26], Simone Aparecida Vieira[27], Luiz Aragão[28], Alejandro Araujo-
463 Murakami[29], Eric J.M.M. Arets[30], Luzmila Arroyo[31], Peter Ashton[32], Gerardo Aymard C.[33], Fabrício B.
464 Baccaro[34], Lindsay F. Banin[35], Christopher Baraloto[36], Plínio Barbosa Camargo[37], Jos Barlow[38], Jorcely
465 Barroso[39], Jean-François Bastin[40], Sarah A. Batterman[1,41,42,43], Hans Beeckman[12], Serge K. Begne[17,44], Amy
466 C. Bennett[44], Erika Berenguer[19,38], Nicholas Berry[45], Lilian Blanc[46], Pascal Boeckx[47], Jan Bogaert[48], Damien
467 Bonal[49], Frans Bongers[50], Matt Bradford[51], Francis Q. Brearley[2], Terry Brncic[52], Foster Brown[53], Benoit
468 Burban[54], José Luís Camargo[26], Wendeson Castro[55], Carlos Céron[56], Sabina Cerruto Ribeiro[57], Victor
469 Chama Moscoso[15], Jerôme Chave[58], Eric Chezeaux[59], Connie J. Clark[25], Fernanda Coelho[1], Murray
470 Collins[61], James A. Comiskey[62,63], Fernando Cornejo Valverde[64], Massiel Corrales Medina[65], Lola da
471 Costa[66], Martin Dančák[67], Greta C. Dargie[1], Stuart Davies[68], Nallaret Davila Cardozo[69], Thales de
472 Haulleville[12,48], Marcelo Brilhante de Medeiros[70], Jhon del Aguila Pasquel[71], Géraldine Derroire[72], Anthony
473 Di Fiore[73], Jean-Louis Doucet[74], Aurélie Dourdain[72], Vincent Droissant[75], Luisa Fernanda Duque[76], Romeo
474 Ekoungoulou[77], Fernando Elias[78], Terry Erwin[79], Adriane Esquivel-Muelbert[80], Sophie Fauset[81], Joice
475 Ferreira[82], Gerardo Flores Llampazo[83], Ernest Foli[84], Andrew Ford[51], Martin Gilpin[1], Jefferson S. Hall[85],
476 Keith C. Hamer[86], Alan C. Hamilton[87], David J. Harris[88], Terese B. Hart[89,90], Radim Hédl[91,92], Bruno
477 Herault[72], Rafael Herrera[93], Niro Higuchi[6], Annette Hladik[94], Eurídice Honorio Coronado[71], Isau
478 Huamantupa-Chuquimaco[95], Walter Huaraca Huasco[95], Kathryn J. Jeffery[96], Eliana Jimenez-Rojas[97],
479 Michelle Kalamandeen[1], Marie-Noel Kamdem[11,13,17,98], Elizabeth Kearsley[99], Ricardo Keichi Umetsu[100], Lip
480 Khoon Kho Khoon[101], Timothy Killeen[102], Kanehiro Kitayama[103], Bente Klitgaard[104], Alexander Koch[105],
481 Nicolas Labrière[58], William Laurance[106], Susan Laurance[106], Miguel E. Leal[107], Aurora Levesley[1], Adriano
482 J. N. Lima[6], Janvier Lisingo[11], Aline P. Lopes[108,109], Gabriela Lopez-Gonzalez[1], Tom Lovejoy[110], Jon
483 Lovett[1], Richard Lowe[111], William E. Magnusson[112], Jagoba Malumbres-Olarte[113,114], Ângelo Gilberto
484 Manzatto[115], Ben Hur Marimon Junior[116], Andrew R. Marshall[8,117,118], Toby Marthews[119], Simone Matias de
485 Almeida Reis[14,19], Colin Maycock[120], Karina Melgaço[1], Casimiro Mendoza[121], Faizah Metali[122], Vianet
486 Mihindou[123,124], William Milliken[104], Edward Mitchard[125], Paulo S. Morandi[14], Hannah L. Mossman[2], Laszlo
487 Nagy[126], Henrique Nascimento[6], David Neill[127], Reuben Nilus[128], Percy Núñez Vargas[95], Walter Palacios[129],
488 Nadir Pallqui Camacho[1,95], Julie Peacock[1], Colin Pendry[130], Maria Cristina Peñuela Mora[131], Georgia C.
489 Pickavance[1], John Pipoly[132], Nigel Pitman[133], Maureen Playfair[134], Lourens Poorter[135], John R. Poulsen[25],
490 Axel D. Poulsen[136], Richard Preziosi[2], Adriana Prieto[137], Richard Primack[138], Hirma Ramírez-Angulo[139], Jan
491 Reitsma[140], Maxime Réjou-Méchain[75], Zorayda Restrepo Correa[141], Thaiane Rodrigues de Sousa[6], Lily
492 Rodriguez Bayona[142], Anand Roopsind[143], Agustín Rudas[137], Ervan Rutishauser[42,144], Kamariah Abu
493 Salim[122], Rafael P. Salomão[145,146], Juliana Schietti[6], Douglas Sheil[147], Richarlly C. Silva[57,148], Javier Silva
494 Espejo[149], Camila Silva Valeria[38], Marcos Silveira[57], Murielle Simo-Droissart[17], Marcelo Fragomeni
495 Simon[70], James Singh[150], Yahn Carlos Soto Shareva[15], Clement Stahl[54], Juliana Stropp[151], Rahayu Sukri[122],
496 Terry Sunderland[152,153], Martin Svátek[154], Michael D. Swaine[155], Varun Swamy[156], Hermann Taedoumg[17],
497 Joey Talbot[1], James Taplin[157], David Taylor[158], Hans ter Steege[159,160], John Terborgh[25], Raquel Thomas[143],
498 Sean C. Thomas[161], Armando Torres-Lezama[162], Peter Umunay[163,164], Luis Valenzuela Gamarra[15], Geertje
499 van der Heijden[165], Peter van der Hout[166], Peter van der Meer[167], Mark van Nieuwstadt[168], Hans Verbeeck[99],
500 Ronald Vernimmen[169], Alberto Vicentini[6], Ima Célia Guimarães Vieira[146], Emilio Vilanova Torre[170], Jason
501 Vleminckx[36], Vincent Vos[172], Ophelia Wang[173], Lee J. T. White[124,174,175], Simon Willcock[176], John T.
502 Woods[177], Virginia Wortel[178], Kenneth Young[179], Roderick Zagt[180], Lise Zemagho[17], Pieter A. Zuidema[50],
503 Joeri A. Zwerts[178,181], Oliver L. Phillips[1]

504

2

Supporting information for Sullivan et al.

505 **This file includes:**

506 Materials and Methods

507 Figures S1 – S15

508 Tables S1 – S2

509

**Materials and Methods**

Forest census data

Our plots come from the RAINFOR, AfriTRON, and T-FORCES networks. Forest inventory plots were located in lowland (<1200 m), old-growth, closed-canopy forests that were not known to have been subject to anthropogenic disturbance through fire or selective logging. Plots characterised floristically as dry forest were not included, as were plots that received less than 1200 mm precipitation each year. We also did not include plots in white sand, swamp and seasonally flooded forests, as we expect these to experience marked edaphic constraints (extreme nutrient limitation for white sand forests (*32*), stress caused by hypoxic conditions for swamp and seasonally flooded forests (*33*)). All plots were ≥ 0.2 ha (median size = 1 ha) and were monitored for at least two years (median monitoring period = 9.7 years). All censuses were prior to the 2015-16 very strong El Niño event, as we expected that event to supress carbon gains relative to the long-term mean.

Forest inventory plots were sampled using standardised protocols (*34*), where all live stems with diameter ≥ 100 mm were measured at 1.3 m or 50 cm above buttresses and deformities. Trees were tagged so that the same tree could be identified in subsequent censuses. In some cases the point of diameter measurement (POM) had to be moved due to upward growth of buttresses and deformities. For these trees we use the $D_{mean}$ approach from Talbot et al. (*35*).

In a few cases (6 plots) the minimum diameter measured changed over time, or palms and *Phenakospermum* were excluded in some censuses. For these, we estimated aboveground biomass (AGB, subsequently converted to carbon stocks) and aboveground woody production (AGWP, subsequently converted to carbon gains) using a minimum diameter or taxonomic protocol that could be consistently applied across censuses, and scaled these values by the aboveground biomass ratio between that protocol and all stems ≥ 100 mm protocol for censuses when all stems were measured. Some plots had nested designs where the plot was split into subplots with different minimum diameter protocols (69 plots). For these, we only analysed the area conforming to our minimum diameter protocol. For analysis, we grouped small (≤ 0.5 ha) plots within 1 km of each other, and also grouped contiguous larger plots (18 plots), as these will experience equivalent climate and larger plots are less sensitive to stochastic tree fall events (*36*).

Data were curated in ForestPlots.net (*37, 38*), or were subject to equivalent offline handling, and experienced the same quality control procedures. Details of quality control procedures are described in Brienen et al. (*39*). Our final dataset consists of 590 sampling units (hereafter plots) covering 637.2 ha, with 2.2 million measurements of 670,499 unique stems. For validating models of carbon stocks an additional dataset of 223 single-census plots using the same measurement protocols was assembled from the same networks (see section "Validation with independent single-census plot dataset" below).

544

<u>545</u>    <u>Estimating above-ground biomass</u>

546    Diameter measurements were converted to estimates of aboveground biomass (AGB). For dicot trees

547    we used the allometric equation

548    AGB = $0.673 \times (\rho D^2 H)^{0.976}$,                                    [1]

549    from Chave et al. (*40*), where $\rho$ is wood density (from (*41, 42*)) and $H$ is tree height estimated using

550    allometric equations described below. For monocots and tree ferns, we used a palm-specific

551    allometric equation

552    ln(AGB) = -3.3488 + 2.7483.ln(*D*),                           [2]

553    from Goodman et al. (*43*), where *D* is the measured diameter.

554    The heights of a subset of trees in our dataset were measured in the field, either with a laser

555    rangefinder, hypsometer, or clinometer, or directly by climbing the tree. We filtered this dataset to

556    stems with measured diameters, height ≤ 90 m, diameters ≥ 90 mm DBH, as height-diameter

557    allometries of saplings differ from those of more mature trees, and to stems that were not broken,

558    leaning or fallen. This gave a total of 78,899 height measurements. We used this dataset to fit local

559    height-diameter allometric models, as these refine AGB estimates by capturing spatial variation in

560    height-diameter allometries missed by large-scale allometric models (*44*). Height data were not

561    available from every plot, so to ensure consistent treatment of plots height-diameter models were

562    constructed for each biogeographic region. We fitted three parameter asymptotic models (*45*) of the

563    form

564    $H = a(1-\exp(-bD^C))$,                                    [3]

565    where *a*, *b* and *c* are estimated parameters ('Weibull' models, *46*). We fitted these models either

566    treating each observation equally or with case weights proportional to each trees' basal area. These

567    weights give more importance to large trees during model fitting. We selected the best fitting of these

568    models, determining this as the model that minimised prediction error of stand biomass when

569    calculated with estimated heights or observed heights (*44*). Weibull models were implemented using

570    the nls function in R with default settings. Starting values of *a* = 25, *b* = 0.05 and *c* = 0.7 were chosen

571    following trial and error as they led to regular model convergence. Where models did not converge

572    this was usually because the height-diameter relationship did not reach an asymptote, so in these cases

573    we used the log-log model ln(*H*) = *a* + *b*(ln(*D*)) to estimate height, where *b* gives the scaling exponent

574    of a power law relationship between height and diameter. We checked if models gave unrealistic

575    predictions by applying models to predict the height of all trees in the biogeographic region, and

576    excluded models that predicted any tree height 10 % higher than the tallest tree we recorded in that

577    continent.

578

579    <u>Estimating above-ground woody production</u>

580    We estimated AGWP following Talbot et al. (*35*). AGWP is comprised of four components, (1) the

581    sum of growth of surviving trees, (2) the sum of AGB of new recruits, (3) the sum of unobserved

582    growth of trees that died during a census interval and (4) the sum of growth of unobserved recruits

583    that entered then died during a census interval. Accounting for the latter two components is necessary

584    to avoid census-interval length effects, as more AGWP in these components will be missed due to the

585    greater mortality of trees that accumulates over longer census intervals.

586    Components 3 and 4 can be estimated using two quantities that can be calculated from observed stem-

587    dynamics in each plot; per-area annual recruitment ($R_a$) and per-capita annual mortality ($m_a$). Per-

588    capita mortality is calculated from the ratio of surviving stems to initial stems, using equation 5 in

589    Kohyama et al. (*47*). Per-area annual recruitment is calculated using estimated mortality rates and the

590    observed change in the number of stems over a census interval, using equation 11 of Kohyama et al.

591    (*47*).

592    To estimate the unobserved growth of stems that died during a census interval, we first use plot-level

593    per-capita mortality rates ($m_a$) to estimate how many trees are expected to have died in each year of

594    the census interval, and from that calculate the mean number of years that trees that died during the

595    census interval would have lived before death. The diameter of tree at death ($D_{death}$) can then be

596    estimated as

597    $D_{death} = D_{start} \times G \times Y_{mean}$                             [4]

598    where $D_{start}$ is the diameter at the start of the census interval, $G$ is the plot-level median growth rate of

599    the size class the tree was in at the start of the census interval (size classes are defined as $D < 200$ mm,

600    $400$ mm $> D \geq 200$ mm, and $D \geq 400$ mm) and $Y_{mean}$ is the mean number of years trees survived in

601    the census interval before dying. The diameter at death is then converted to AGB at death using

602    allometric equations (equation 1, except for ferns and monocots where equation 2 is used), and the

603    unobserved growth is calculated as the difference between AGB at death and AGB at the start of the

604    census.

605    To estimate the growth of recruits that were not observed because they died during the census

606    interval, we first need to estimate the number of unobserved recruits. This can be estimated from per-

607    area annual recruitment ($R_a$) and per-capita annual mortality ($m_a$): $R_a$ gives the number of stems per ha

608    that recruit in a given year, and the probability of each recruit surviving until the next census ($P_{surv}$) is

6

609     $P_{surv} = (1\text{-}m_a)^T$, where $T$ is the number of years remaining in the census interval. The number of

610     recruits in a given year that survive to the next census is $R_a - P_{surv}R_a$. Summing this for each year in a

611     census interval gives the total number of unobserved recruits in that census interval. We then need to

612     estimate how long each recruit was alive for. From $m_a$ we can calculate the number of recruits in a

613     given year that died in each subsequent year, and from this calculate the mean life-span of recruits in a

614     given year that died before the next census. The average life-span of unobserved recruits ($Y_{mean\text{-}rec}$) is

615     the weighted mean of each cohort's lifespan, weighted by the number of unobserved recruits in each

616     year. Diameter at death is given in mm by

617     $D_{\text{death}} = 100 + (G \times Y_{mean\text{-}rec})$                               [5]

618     where $G$ is the plot-level median growth rate of the smallest size class (i.e. $D < 200$ mm).

619     Aboveground biomass of recruits at the time of death is estimated using equation 1. These corrections

620     for unobserved growth have a marginal impact on AGWP calculations, collectively accounting on

621     average for just 2.3 % of estimated plot-level AGWP.

622     AGB was calculated for each census, and AGWP was calculated for each census interval, and the

623     time-weighted mean of each was taken to give one value per plot. We used a time-weighted mean to

624     give greater importance to AGB estimates separated by longer census-intervals, as these will be more

625     independent. Estimates of AGB and AGWP were converted to carbon stocks and carbon gains by

626     multiplying by 0.456 (*48*). Carbon residence time was then estimated as carbon stocks /carbon gains,

627     and represents the length of time carbon resides in living biomass before being passed to the litter and

628     necromass pools (*49*). Calculations to estimate AGB and AGWP were performed using the R package

629     BiomasaFP (*50*).

630

631     <u>Obtaining environmental data</u>

632     Most climate data were obtained from climate data from Worldclim2 (*51*) as it provides the highest

633     resolution (~ 1 km) pantropical climate data, although we note that some regions, such as central

634     Africa, have limited station data. We extracted monthly data for the following variables: mean daily

635     minimum temperature, mean daily maximum temperature, precipitation, solar radiation and wind

636     speed, In addition to calculating the standard series of 19 bioclimatic variables, using the dismo R

637     package (*52*), we calculated 1) mean daily maximum temperature, BIO1 + BIO2/2, 2) mean daily

638     minimum temperature, BIO1 – BIO2/2, 3) maximum cumulative water deficit as the minimum across

639     the year of monthly cumulative water deficit $W$,

640     $W_i = W_{i\text{-}1} - \min(0, P_i - 100)$ ,                               [6]

641    where $P$ is monthly precipitation in mm, and 100 represents measured evapotranspiration. This

642    calculation was run for a year from the wettest month in the year, starting at a water deficit of zero, 4)

643    the number of months where monthly cumulative water deficit was negative, 5) the number of months

644    where monthly precipitation was below 100 mm (i.e. less than evapotranspiration), 6) mean annual

645    solar radiation, 7) mean annual wind speed, and 8) vapour pressure deficit (VPD = SVP – vapour

646    pressure, where saturated vapour pressure, SVP, $= 0.611 \times e^{(17.502\ temperature)\ /\ (temperature\ +\ 240.97)}$). We also

647    obtained data on cloud frequency at ~1 km resolution from Wilson & Jetz (*53*), who processed twice-

648    daily MODIS satellite images. Temperature values were adjusted for differences in altitude between

649    the plot and the 1 km grid cell used for Worldclim interpolation, as these can differ in topographically

650    diverse regions, using lapse rates, so that $T_{plot} = T_{worldclim} + 0.005 \times (A_{worldclim} - A_{plot})$, where $T$ is

651    temperature (°C) and $A$ is altitude (m). Temperature values were also corrected for systematic

652    warming trends. To do this, the mean annual temperature in each grid-cell in each year was extracted

653    from the CRU TS 3.24 dataset (*54*), and robust linear regression used to estimate grid-cell specific

654    warming rates. These were used to adjust Worldclim2 temperature values for the difference between

655    the midpoint of plot monitoring and the midpoint of the Worldclim2 climatology.

656    Data on soil texture and chemistry was obtained at 1 km resolution from the SoilGrids dataset (*55*),

657    with this resolution selected to match the resolution of the climate data. From this we extracted CEC,

658    representing soil fertility, and percentage clay, representing soil texture. For each soil variable we

659    calculated the depth-weighted average for 0 – 30 cm.

660    <u>Statistical analysis</u>

661    We used linear models to relate carbon, carbon gains and carbon residence time to environmental

662    explanatory variables. The role of different explanatory variables was assessed using multi-model

663    inference.

664    Response variables were positively skewed and had positive mean-variance relationships, so were

665    log-transformed to meet the assumption of normality and reduce heterogeneity in variances. The log-

666    normal nature of forest carbon stocks and dynamics means that there is greater potential for variation

667    when forests are large, which could be due to the non-linear scaling of tree biomass and tree basal

668    area.

669    We selected explanatory variables to represent hypothesised ways in which climate could affect

670    carbon stocks (Table S1). We assessed colinearity within this set of explanatory variables using

671    variance inflation factors (VIF) and pairwise correlations. Because of colinearity, we had to exclude

672    VPD, total precipitation, use only one of MCWD and precipitation in the driest quarter, and could

673    include both minimum and maximum temperature but not mean annual temperature. We used

674    precipitation in the driest quarter rather than MCWD as the latter is zero truncated and so is less

675    amenable to regression analysis. After removing these variables all pairwise correlations (including

676 with soil explanatory variables) were weak enough not to cause problems through collinearity ($r < 0.6$

677 and VIF $< 3$).

678 To account for variation other than in climate we also included soil variables relating to texture (%

679 clay) and fertility (CEC), and included continent specific intercepts to account for biogeographic

680 variation in carbon. To account for unmeasured environmental gradients (e.g. soil variation not

681 captured by the SoilGrids variables), we used Moran's eigenvector maps as explanatory variables,

682 selecting eigenvectors the corresponded to positive spatial autocorrelation in the distance matrix (*56*).

683 These variables act as a proxy for unmeasured spatial gradients by capturing positive spatial

684 associations between plots.

685 Plots differed in their area and the length of time they were monitored for. This is likely to affect the

686 variance of carbon stocks, carbon gains and carbon residence time, as smaller plots or plots only

687 monitored for short periods are more likely to be sensitive to the mortality of a few large trees. To

688 account for this, we used case weights relating to plot area and monitoring period. Following Lewis et

689 al. (*57*), we selected weights by relating residuals from our linear models to plot area and to plot

690 monitoring period, and subsequently assessing which root transformation of plot area/ monitoring

691 period removed the pattern in the residuals when used as a weight. Selected weights were: carbon

692 stocks, Area $^{1/3}$; carbon gains, Monitoring length $^{1/7}$; carbon residence time, Area $^{1/9}$ + Monitoring

693 length $^{1/12}$ -1.

694 We fitted all subsets of the general linear model with explanatory variables described above, forcing

695 spatial eigenvectors into all models. We then averaged the subset of models where $\Delta$ AIC $< 4$, using

696 full averaging so variables that do not appear in the model get the value of zero for their coefficients.

697 This means that model averaged coefficients of terms with limited support exhibit shrinkage towards

698 zero. Multi-model inference was performed using the MuMIn R package (*58*).

699 We assessed whether the two climate variables found to have important additive effects on carbon

700 stocks in this analysis (mean daily maximum temperature in the warmest month and precipitation in

701 the driest quarter) interacted with each other by adding an interaction term between these variables to

702 the full generalised linear model of carbon stocks as a function of other climate and soil variables,

703 continent and spatial eigenvectors. We compared these two models using AIC. We repeated this with

704 carbon gains and carbon residence time as response variables.

705 To assess whether the temperature carbon relationship was non-linear we used breakpoint regression

706 implemented in the segmented R package (*59*). This estimates a breakpoint in the explanatory variable

707 at which the slope of the relationship with the response variable changes. We estimated the breakpoint

708 for the mean daily maximum temperature in the warmest month variable in the full model with a

709 temperature-precipitation interaction described above. We assessed the support for the breakpoint by

9

710   comparing the AIC of the model with a breakpoint with the AIC of a model with a linear relationship.

711   We repeated this with carbon gains and carbon residence time as response variables.

712   We also analysed spatial variation in carbon stocks as a function of the above climate and soil

713   variables and spatial eigenvectors using Random Forest decision tree algorithms (*22*) implemented

714   using the randomForest R package (*60*). We assessed variable importance by calculating the average

715   increase in node purity across all decision trees (measured by residual sum of squares) when using the

716   variable to split the data. We assessed modelled relationships between response and explanatory

717   variables using partial plots, which show predicted change in the response variable, averaged across

718   trees, when changing the explanatory variable and holding all other variables constant.

719   To compliment this analysis based on relationships expected *a priori*, we also performed an

720   exploratory analysis to assess whether other climate variables excluded from the full general linear

721   models had an effect on carbon. To do this, we fitted linear models to assess the bivariate relationship

722   of carbon with each climate variable, with continent also included as an explanatory variable to

723   account for biogeographic variation in forest characteristics.

724

725   <u>Validation with independent single-census plot dataset</u>

726   We assessed whether the relationships with environmental variables identified in the analyses of

727   multi-census plot data described above held when applied to an additional dataset of 223 single-

728   census plots. As the single-census data were not used in any of the analyses above they did not

729   influence modelling decisions, so provide an independent test of the relationships identified with the

730   multi-census plot analysis.

731   Single-census plots were extracted from the ForestPlots.net database (*37, 38*) using the same plot-

732   selection criteria as for the multi-census plots, except that censuses during or following the 2015-16

733   strong El Niño were included in the single-census plot dataset as we expected that carbon stocks,

734   unlike gains, would still remain close to their long-term mean.

735   We fitted a general linear model with the five climate explanatory variables, soil fertility and texture,

736   continent and spatial eigenvector, and model averaging of all subsets of this model as described for

737   the multi-census plots. We performed this analysis using just the single-census plots and a combined

738   dataset of single and multi-census plots.

739

740

741

10

742    <u>Scaling results to the biome</u>

743    We applied the non-linear relationship between carbon stocks and mean daily maximum temperature

744    in the warmest month identified by the breakpoint regression to estimate the total change in carbon

745    stock due to temperature effects alone for different scenarios of temperature increase. We delimited

746    the biome extent using the WWF tropical and subtropical moist broadleaved forest biome (*61*),

747    restricted to tropical latitudes, and further refined it by excluding grid-cells with $< 50$ Mg C ha$^{-1}$ using

748    data from (*30*), as these are unlikely to be forest. Calculations were conducted at 10-minute

749    resolution. The non-linear relationship between temperature and carbon means that the change in

750    biomass for a given increase in temperature will depend on the baseline temperature. For each grid-

751    cell we predicted the percentage change in carbon for a given temperature increase from the baseline

752    temperature in that grid-cell based on the non-linear relationship identified in our statistical model,

753    holding all other variables constant. We then used a reference carbon stock map (*30*) to convert

754    percentage change to change in carbon stocks per hectare (in Mg ha$^{-1}$). To calculate change in carbon

755    stocks for the whole grid-cell, we multiplied change per hectare by the area of the grid-cell in

756    hectares, and then adjusted this by the proportion of the grid-cell that was forested by multiplying by

757    2014 forest cover (*62*). Total change for the biome (in Pg) was calculated by summing these grid-cell

758    level values. Uncertainty due to our statistical model was assessed by generating multiple predictions

759    by resampling model parameters (breakpoint threshold, slope below breakpoint, slope above

760    breakpoint), and extracting quantiles from the resultant distribution of predicted change values.

761    Aboveground biomass carbon values were scaled to include root biomass based on a root to shoot

762    ratio of 0.19 in tropical evergreen forests (*63*).

763    The Avitabile et al (*30*) aboveground biomass map was chosen to provide reference carbon stocks.

764    While other maps have previously been produced by Saatchi et al. (*64*) and Baccini et al. (*65*) we

765    selected the Avitabile map because it synthesises the earlier maps (see Mitchard et al. (*66*) for

766    discussion of substantial differences between these maps) and is anchored by more field data.

767    Importantly, the Avitabile map reproduces spatial patterns in aboveground biomass that have been

768    described from field data but are absent in the Saatchi or Baccini maps, including the much higher

769    biomass density of north-east Amazonian forests due to tall trees and very high wood density (*67*).

770    Nevertheless, we also investigated the consequences of using the Saatchi or Baccini maps for our

771    estimates of biomewide thermal sensitivity and spatial patterns of change in carbon stocks (Fig S15).

772    We investigated three temperature change scenarios. Firstly, we applied a 1°C increase to all

773    locations. Secondly, we assessed the consequence of global temperatures stabilizing 1.5°C above pre-

774    industrial levels for the equilibrium temperature response of tropical forest carbon. Finally, we

775    assessed the consequence of global temperatures stabilizing 2°C above pre-industrial levels. For the

776    latter two we obtained data from CMIP5 climate models, using downscaled future climate projections

11

777    based on the Worldclim climatology (*68*). As downscaling was performed using Worldclim version

778    1.4 (*69*) and our statistical models use Worldclim version 2, we calculated the warming anomaly in

779    each grid-cell from the current Worldclim version 1.4 conditions, and applied this to the Worldclim 2

780    data to obtain future temperature. RCP scenarios and time-points were chosen to give global

781    temperature increases that best match 1.5°C and 2°C above pre-industrial. Importantly, these future

782    climate projections were used to capture the spatially varying nature of warming, and our predictions

783    relate to the long-term response of vegetation if the climate stabilised at these new warming levels,

784    rather than being predictions of transient responses at these specific time-points. For 1.5°C we used

785    RCP 2.6 averaged for 2040-2060 (median temperature increase across models = 1.5°C, (*70*)). For

786    2°C, we used RCP 2.6 averaged for 2040-2060 (median temperature increase models = 1.9°C (*70*)).

787    Note that predicted increases in maximum temperatures were often considerably greater than the

788    global increase, especially in South America. For both scenarios we used the median predicted

789    temperature change for each grid-cell from an ensemble of 15 models (BCC-CSM1-1, CCSM4,

790    CNRM-CM5, GFDL-CM3, GFDL-ESM2G, GISS-E2-R, HadGEM2-AO, HadGEM-ES, IPSL-

791    CM5A-LR, MIROC-ESM-CHEM, MIROC-ESM, MIROC5, MPI-ESM-LR, MRI-CGCM3,

792    NorESM1-M).

793    We assessed the potential for long-term carbon dioxide growth stimulation to offset these long-term

794    temperature effects. We used $CO_2$ concentrations from the RCP scenarios and time-points described

795    above, which approximate the long-term concentrations if the climate stabilised at the new

796    temperatures (*71*). Thus the 1.5°C and 2°C scenarios were associated with $CO_2$ concentrations of 443

797    ppm and 487 ppm respectively (*72*). We cannot assess the effect of $CO_2$ on biomass from our spatial

798    dataset, so instead used independent estimates of $CO_2$ effects from other sources. Firstly, we obtained

799    $CO_2$ only effects on net primary production (NPP) extracted from an ensemble of CMIP5 earth system

800    models by (*73*). This gives the proportional change in NPP for evergreen forests (note that this also

801    includes boreal forests) over 1980-2010, standardised to a 100 ppm increase in $CO_2$ concentration. To

802    propagate this through to changes in AGB under future $CO_2$ conditions we first estimated the

803    logarithmic dependency of NPP on $CO_2$ (*74*) by substituting values of NPP and $CO_2$ at time zero and *t*

804    (from (*73*)) into the equation,

805    $$NPP_t = NPP_0 \left[ 1 + \beta \ln\left(\frac{[CO_2]_t}{[CO_2]_0}\right) \right]$$    Equation 7

806    This equation can be used to compute NPP annually given an initial NPP estimate and a time series of

807    atmospheric $CO_2$ concentrations (from a combination of the observed record from pre-industrial and

808    the RCP 4.5 scenario, modified so that it stabilises at 487 or 443 ppm depending on warming

809    scenario). Initial pre-industrial NPP was back-calculated from present-day values using Equation 7,

810    with 13.3 Mg C ha$^{-1}$ yr$^{-1}$ (mean of nine Amazon plots where NPP has been measured, from (*75*)) used

811    for present-day NPP. To propagate NPP into change in woody biomass (following (*49*)) we used the

812    equation

813    $$\frac{dM_{\text{wood}}}{dt} = \alpha_{\text{wood}} N_{\text{P}} - \frac{M_{\text{wood}}}{\tau_{\text{wood}}}$$        Equation 8

814    where $M_{wood}$ is woody biomass, $N_p$ is NPP, $\alpha_{wood}$ is the allocation of NPP to wood (taken as 0.33, the

815    mean value across nine plots from (*75*)) and $\tau_{\text{wood}}$ is the residence time of woody biomass, taken as

816    59.1 years (the median value across plots used in this study). This model (equations 7 and 8) was run

817    from pre-industrial to 2500, enabling us to see the equilibrium effect of increased $CO_2$ concentrations

818    on biomass, assuming temporally invariant allocation and residence time. We calculated the

819    proportional change in biomass from 2000 to 2500, and applied this to the reference carbon stock map

820    to obtain predicted equilibrium change in aboveground biomass due to $CO_2$ effects.

821    The effects of $CO_2$ in earth system models have been reported to be larger than those deduced from

822    satellite data or $CO_2$ enrichment experiments (*73*), so we also ran the above model using changes in

823    NPP reported from a synthesis of free-air $CO_2$ enrichment experiments conducted in forests (*73*).

824    Finally, we looked at the impact of using $CO_2$ effects derived from a recent large meta-analysis of

825    $CO_2$ enrichment experiments (*76*), which reported a 12.5 % increase in biomass of tropical trees for a

826    250 ppm increase in $CO_2$ concentration. As this relationship was reported to be linear (*76*) we used

827    linear interpolation to estimate the change in biomass under $CO_2$ concentrations associated with each

828    warming scenario (i.e. 443 and 487 ppm). To estimate long-term changes in biomass accounting for

829    both temperature and carbon dioxide, we first applied the $CO_2$ relationship to estimate the change in

830    biomass due to carbon dioxide growth stimulation, and then assessed the effects of warmer

831    temperatures from this revised baseline. Our approach allows a simple assessment of $CO_2$ effects

832    exploring a range of different effect strengths. Real-world responses will likely be more complex,

833    with, for example, nutrient limitation potentially affecting the extent to which growth is stimulated by

834    $CO_2$ (*76*).

835    <u>Temperature sensitivity of CMIP5 models</u>

836    The temperature sensitivity ($\gamma_{LT}$) of coupled climate carbon cycle models can be identified by

837    comparing responses of carbon stocks in coupled and uncoupled simulations forced with a 1%

838    increase in $CO_2$ concentrations per year (respectively, these are the 1pctCO2 and esmFixClim

839    simulations), following Wenzel et al. (*77*). Both coupled and uncoupled simulations are exposed to

840    the same increase in $CO_2$ concentration, but in the uncoupled simulation temperature is not directly

841    affected by this increase in $CO_2$.

842    Vegetation carbon outputs are reported from six CMIP5 models, each with coupled and uncoupled

843    simulations (*78, 79*). For all simulations, we calculated the change in vegetation carbon (the *cVeg*

13

844    variable) in the tropics between year 110 and year 30 of the experiment, and also calculated the

845    difference in land temperature (the *tas* variable). The change in vegetation carbon due to temperature

846    alone was calculated by taking the difference in change in vegetation carbon in the coupled ($\Delta Cveg_C$)

847    and uncoupled ($\Delta Cveg_U$) simulation, and this was then divided by the change in tropical land

848    temperature ($\Delta T$) to obtain the temperature sensitivity of the model,

849    $\gamma_{LT} = (\Delta Cveg_C - \Delta Cveg_U) / \Delta T$                                 Equation 9.

850    We calculated the temperature sensitivity of the six CMIP5 models that report vegetation carbon:

851    CESM-1-BGC ($\gamma_{LT}$ = -0.7 Pg C °C$^{-1}$), GFDL-ESM2M ($\gamma_{LT}$ = -58.4 Pg C °C$^{-}$1), HadGEM2-ES ($\gamma_{LT}$ = -

852    9.2 Pg C °C$^{-1}$), IPSL-CM5A-LR ($\gamma_{LT}$ = -11.3 Pg C °C$^{-1}$), MPI-ESM-LR ($\gamma_{LT}$ = -22.8 Pg C °C$^{-1}$) and

853    NorESM1-ME ($\gamma_{LT}$ = -1.0 Pg C °C$^{-1}$). Note that the simulations do not run to equilibrium (*77*), so

854    changes in carbon stocks due to increased temperature may not be fully realised.
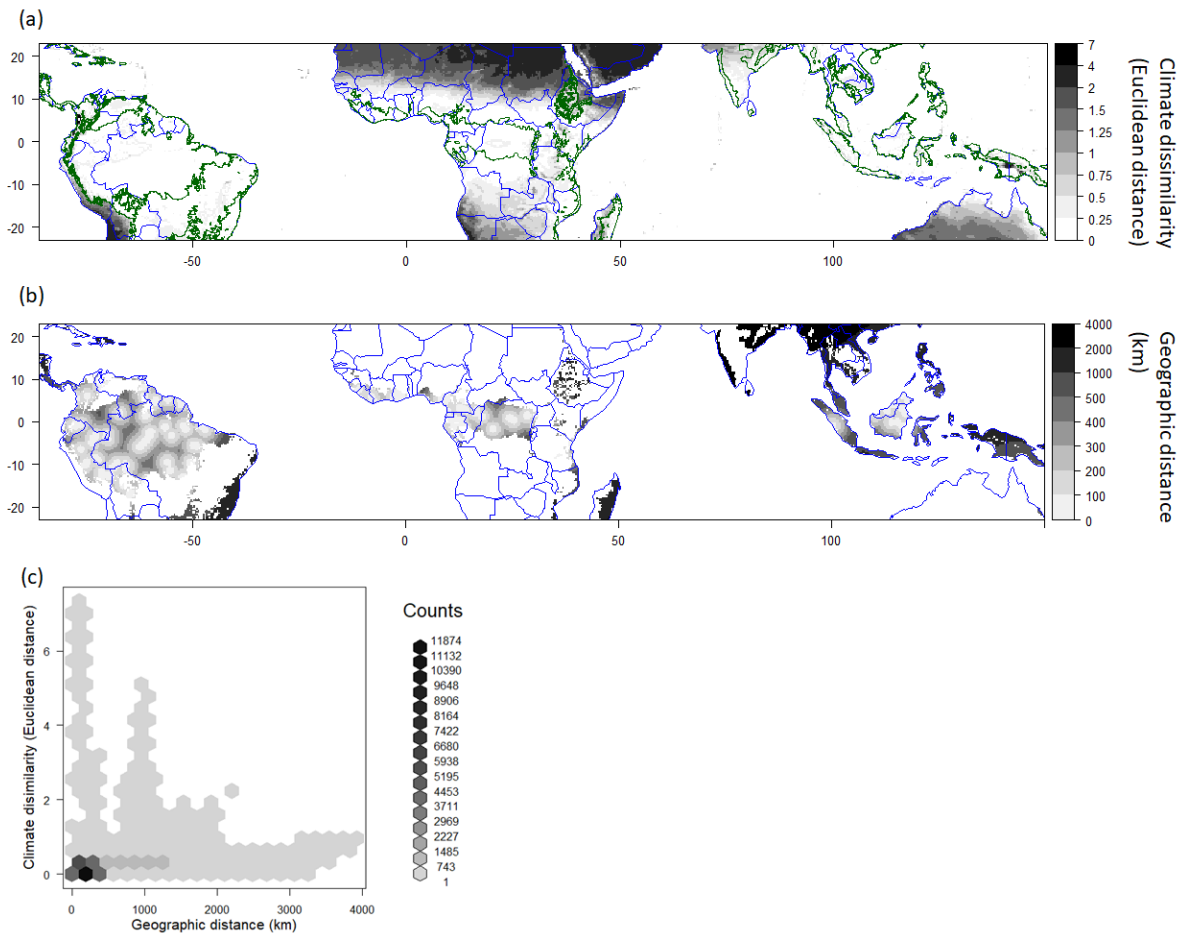
855
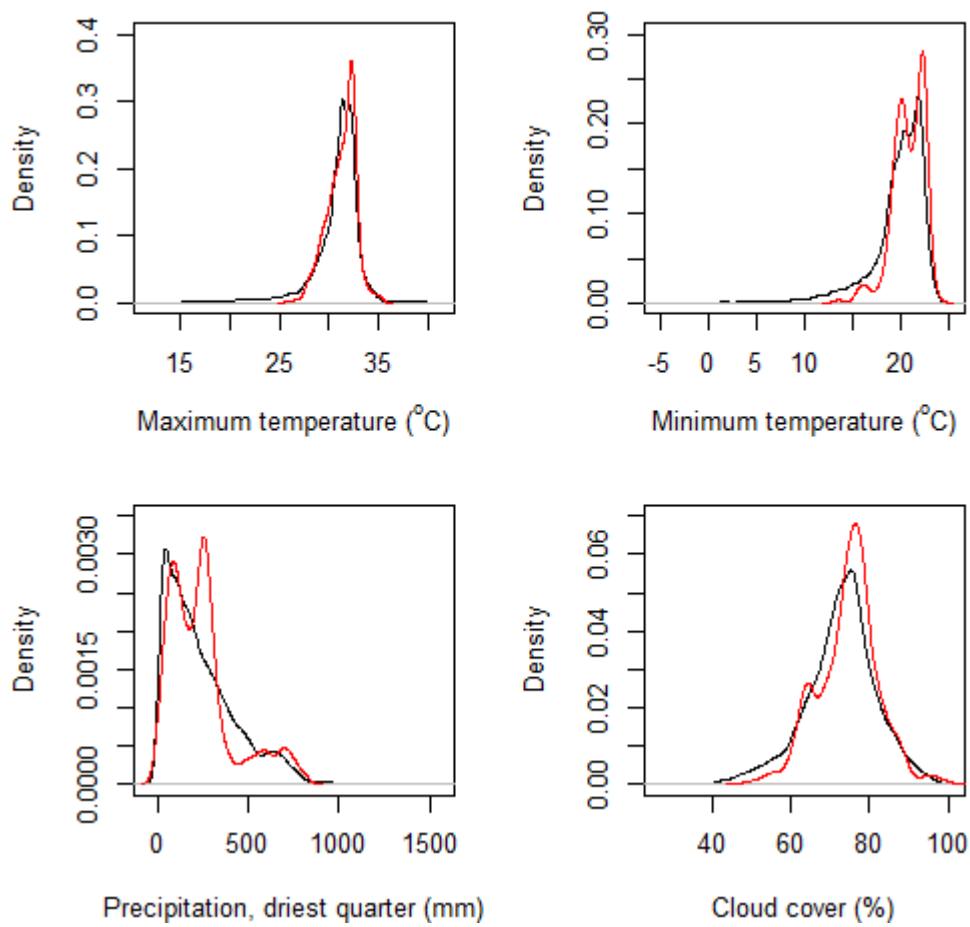
856

857  **Figure S1.** Climate space represented by our plot network. Red lines show the probability density

858  function of each variable in our multi-census plot network. Black lines show the probability density

859  across 10 minute grid-cells in the biome, restricted to areas with forest cover in GLC 2000 (*80*).

860

15

861



862

**Figure S2.** Ability of our plot network to represent the climate conditions found in the moist tropical forest biome. (a) Minimum climate dissimilarity (measured as Euclidean distance on variables scaled by their standard deviation). Climate variables used are the same as in Fig. 2) between 10 minute grid cells and the multi-census plot network. Green lines indicate the extent of the biome. (b) Geographic distance (km) between grid cells and the multi-census plot network. (c) Relationship between climatic and geographic distance of 10 minute grid cells across the tropical forest biome to our plot network. The lack of relationship between climate dissimilarity and geographical distance, alongside the mostly low climatic dissimilarities, shows that our sampling is sufficient to capture the environmental space of the biome and that we can reasonably extrapolate to geographically distant areas from our plots, which are in any case largely deforested already and hence contribute very little to our projected biome-wide carbon response to climate change. (These tropical moist forest areas that are poorly sampled and largely lost include the Atlantic Forests in Brazil, Andean Forests in western South America, eastern Caribbean, Madagascar, and much of tropical South Asia, south China, continental Southeast Asia, Philippines, Sumatra and Java).

877



878
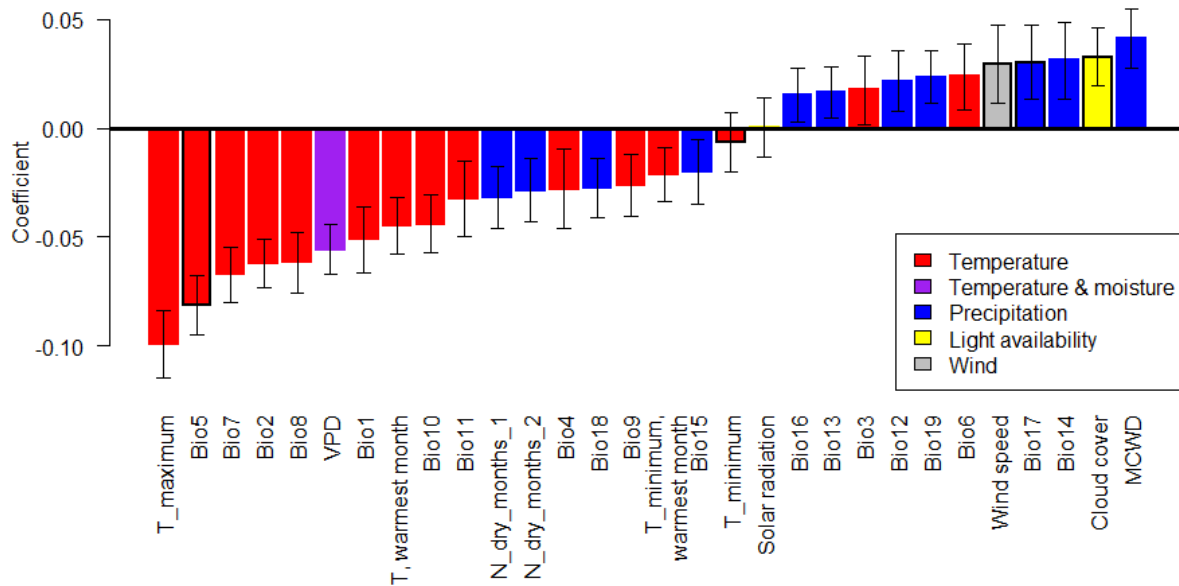
879 **Figure S3.** Relationships between individual climate variables and tropical forest aboveground carbon
880 stocks. Standardised coefficients are from models with the climate variable and continent as
881 explanatory variables and show change in ln(carbon) for a standard deviation change in the
882 explanatory variable. Error bars show standard errors. Variables used in the main analysis have black
883 outlines. Full variable names are: T_maximum – mean daily maximum temperature, Bio5 – mean
884 daily maximum temperature in the warmest month, Bio7 – annual temperature range, Bio2 – mean
885 diurnal temperature range, Bio8 – mean temperature in the wettest quarter, VPD – vapour pressure
886 deficit, Bio1 – mean annual temperature, Bio10 – mean temperature in the warmest quarter, Bio11 –
887 mean temperature in the coldest quarter, N_dry_months_1 – number of months with negative
888 cumulative water deficit, N_dry_months_2 – number of months where precipitation is less than
889 evapotranspiration, Bio4 – temperature seasonality, Bio18 – precipitation in the warmest quarter, Bio9
890 – mean temperature in the driest quarter, T_minimum warmest month – mean daily minimum
891 temperature in the warmest month, Bio15 – precipitation seasonality, T_minimum – mean daily
892 minimum temperature, Bio16 – precipitation in the wettest quarter, Bio13 – precipitation in the
893 wettest month, Bio3 – isothermality, Bio12 – annual precipitation, Bio19 – precipitation in the coldest
894 quarter, Bio6 – mean daily minimum temperature in the coldest month, Wind speed – mean daily
895 wind speed, Bio17 – precipitation in the driest quarter, Bio14 – precipitation in the driest month,
896 Cloud cover – proportion of MODIS passes with cloud present, MCWD – maximum cumulative
897 water deficit (note this is negative when water deficit is high, so a positive relationship with MCWD
898 indicates higher carbon when water deficits are less).

899

900

901

1
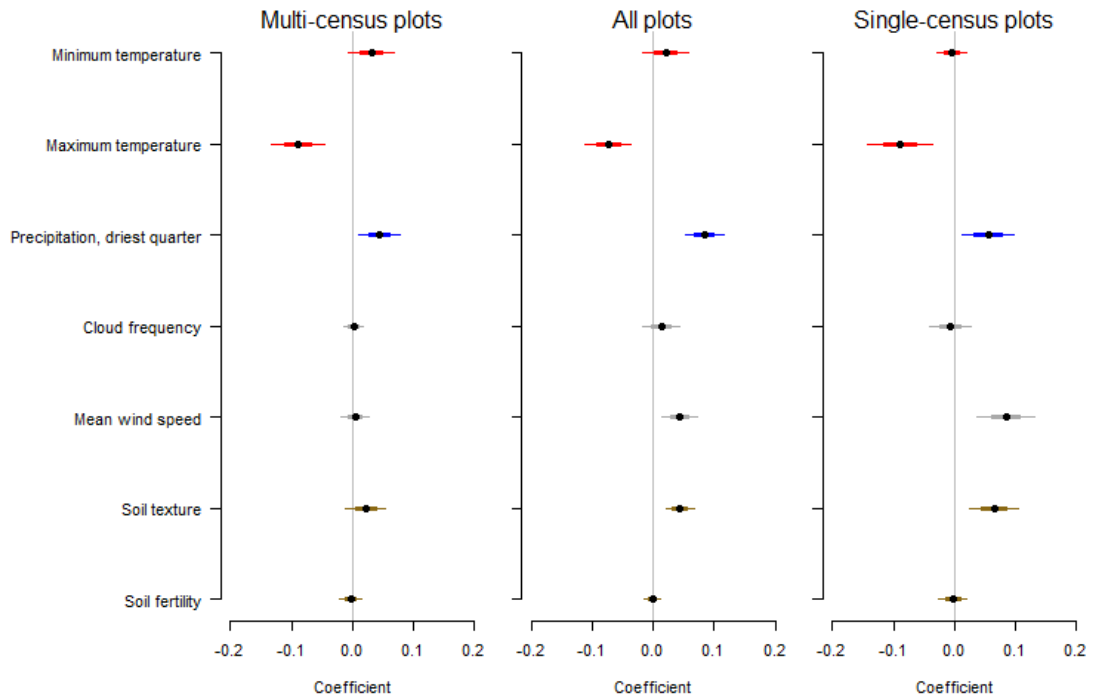
**Figure S4.** Validation of tropical forest carbon stock sensitivity model against an independent dataset of 223 single-census plots from our networks measured with the same protocols. Model-averaged shrinkage adjusted coefficients from multiple regression models of biomass carbon stocks as a function of climate, soil, biogeography and spatial eigenvectors. Models were either fitted to the multi-census plot dataset (as in Fig. 2), to the single-census plot dataset, or to the combined dataset. This analysis shows that the relationships identified to be most important in the main multi-census plot analysis (i.e. the negative relationship between carbon stocks and maximum temperature and positive relationship with precipitation in the driest quarter) are also found in an independent dataset, which was not used for preliminary analysis so did not influence the choice of explanatory variables.

2
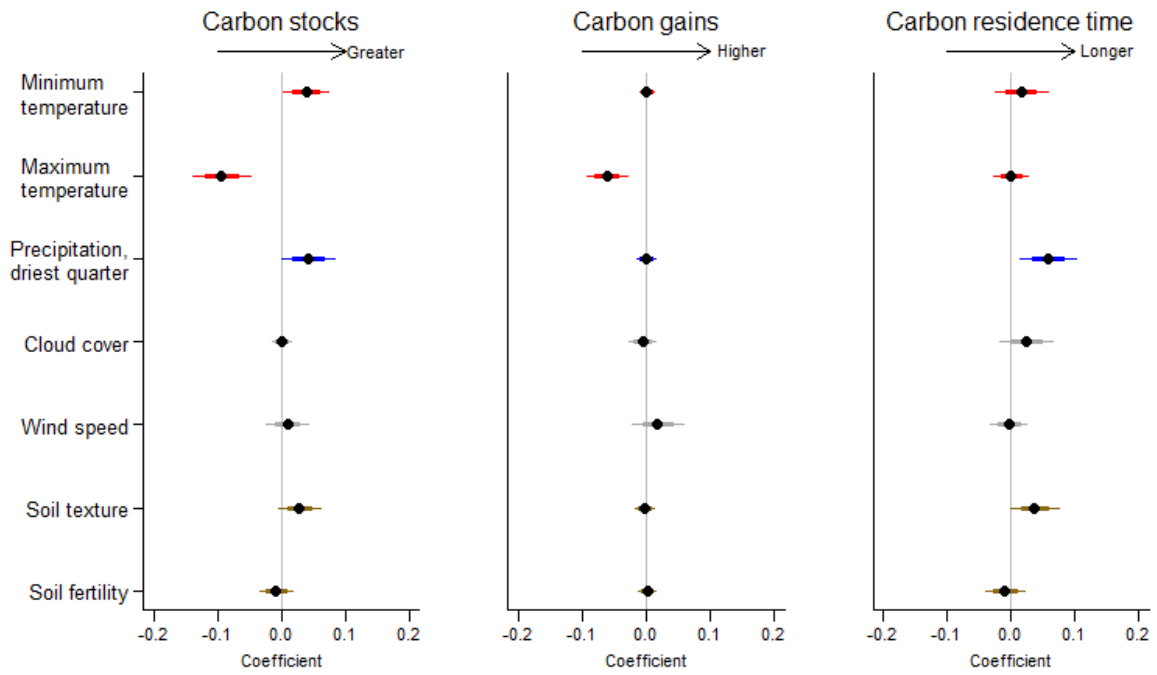
**Figure S5.** As Figure 2, but with aboveground biomass estimated using the Chave et al. 2005 (*81*) moist forest allometric equation, which does not include a height term and is instead based on a third-order polynomial relationship between diameter and aboveground biomass. This indicates that our results are robust to using an alternative allometry to estimate aboveground biomass.

919

920



921
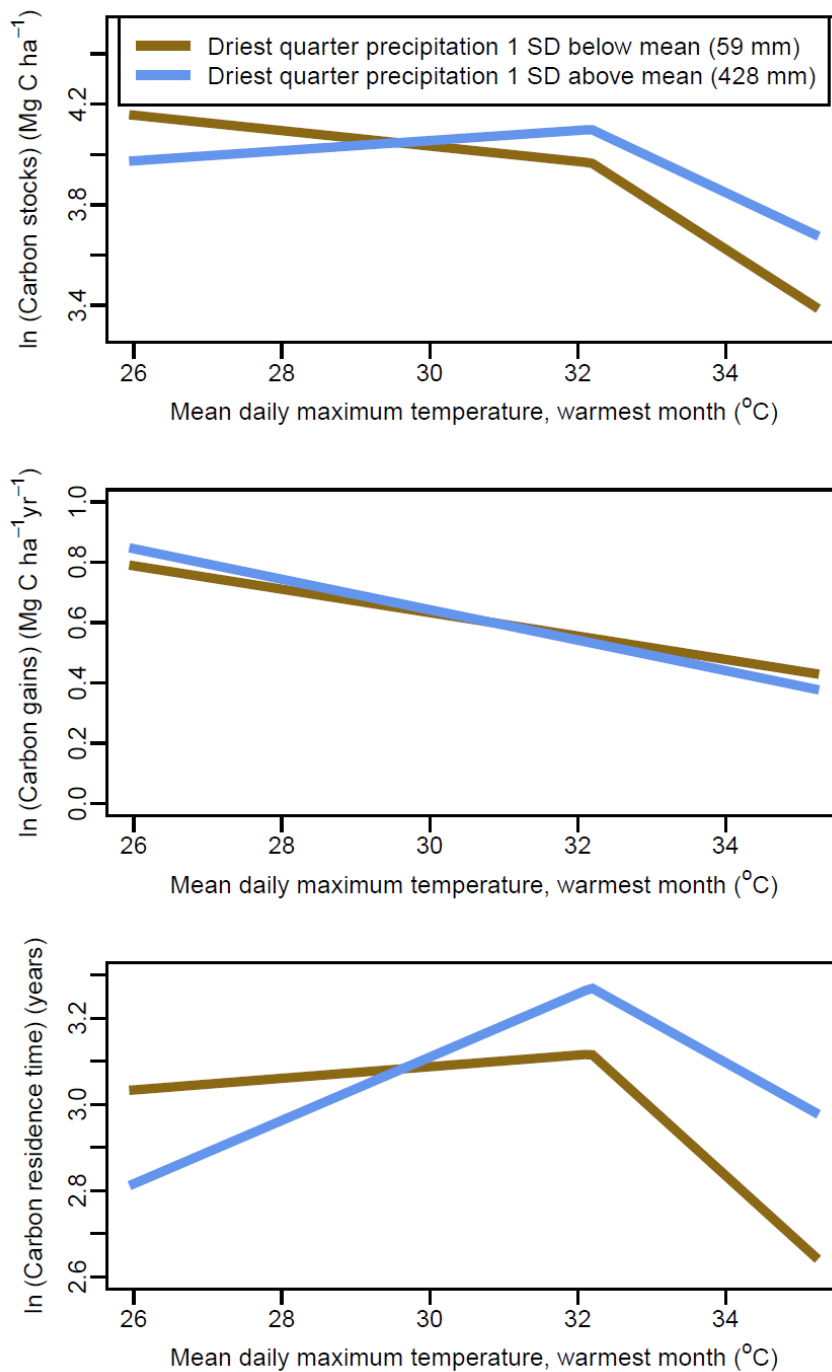
**Figure S6.** Interaction between mean daily maximum temperature in the warmest month and precipitation in the driest quarter in determining aboveground tropical forest carbon stocks, gains and residence time. Modelled relationships with temperature are shown holding precipitation either one standard deviation above or below the mean. Models with breakpoints are shown for carbon stocks and residence time as they were found to be better supported based on lower AIC ($\Delta$AIC >2). Note that the temperature-carbon relationship is steeper when precipitation is low for carbon stocks and (above the breakpoint threshold) carbon residence time, but does not change with precipitation for carbon gains. Response curves are predicted with continent set as Africa.

930     4
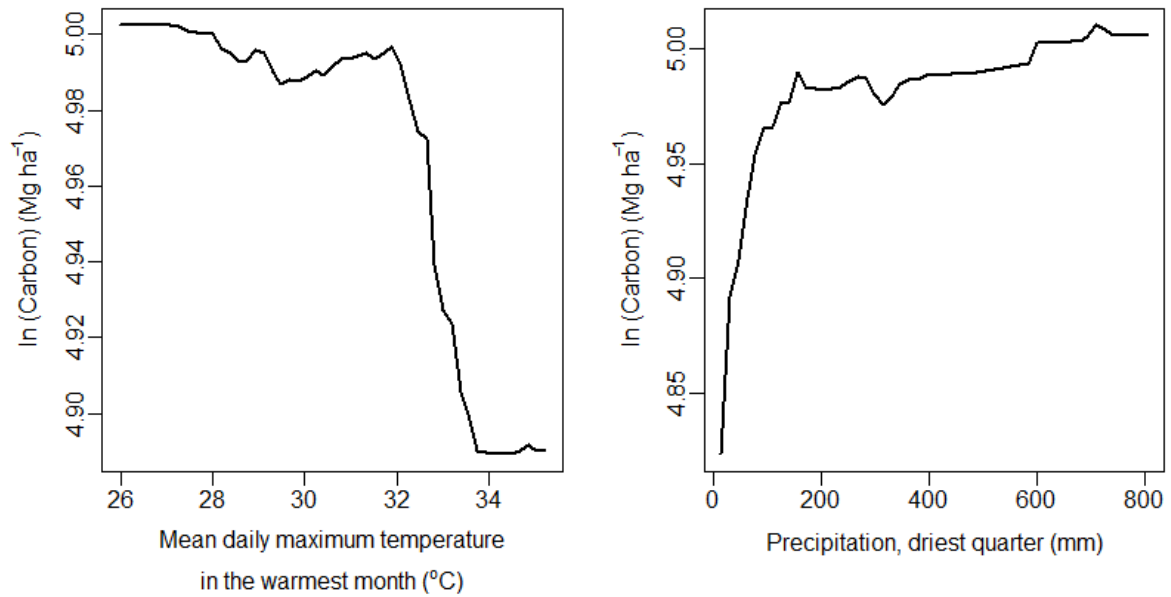
931

932 **Figure S7.** Partial relationships between tropical forest carbon stocks and the two climate variables
933 identified to be most important by the random forest decision tree algorithm. Partial plots show
934 predicted values of carbon stocks averaged across an ensemble of decision tree models when
935 changing the explanatory variable of interest and holding other variables constant. The importance of
936 variables in random forest analysis is assessed by calculating the average increase in node purity
937 across all decision trees (measured by residual sum of squares) when using the variable to split the
938 data. Higher values indicate greater importance. Maximum temperature increased node purity by 4.8
939 and precipitation by 4.7. For all other climate variables increases in node purity were $< 3.5$.

940
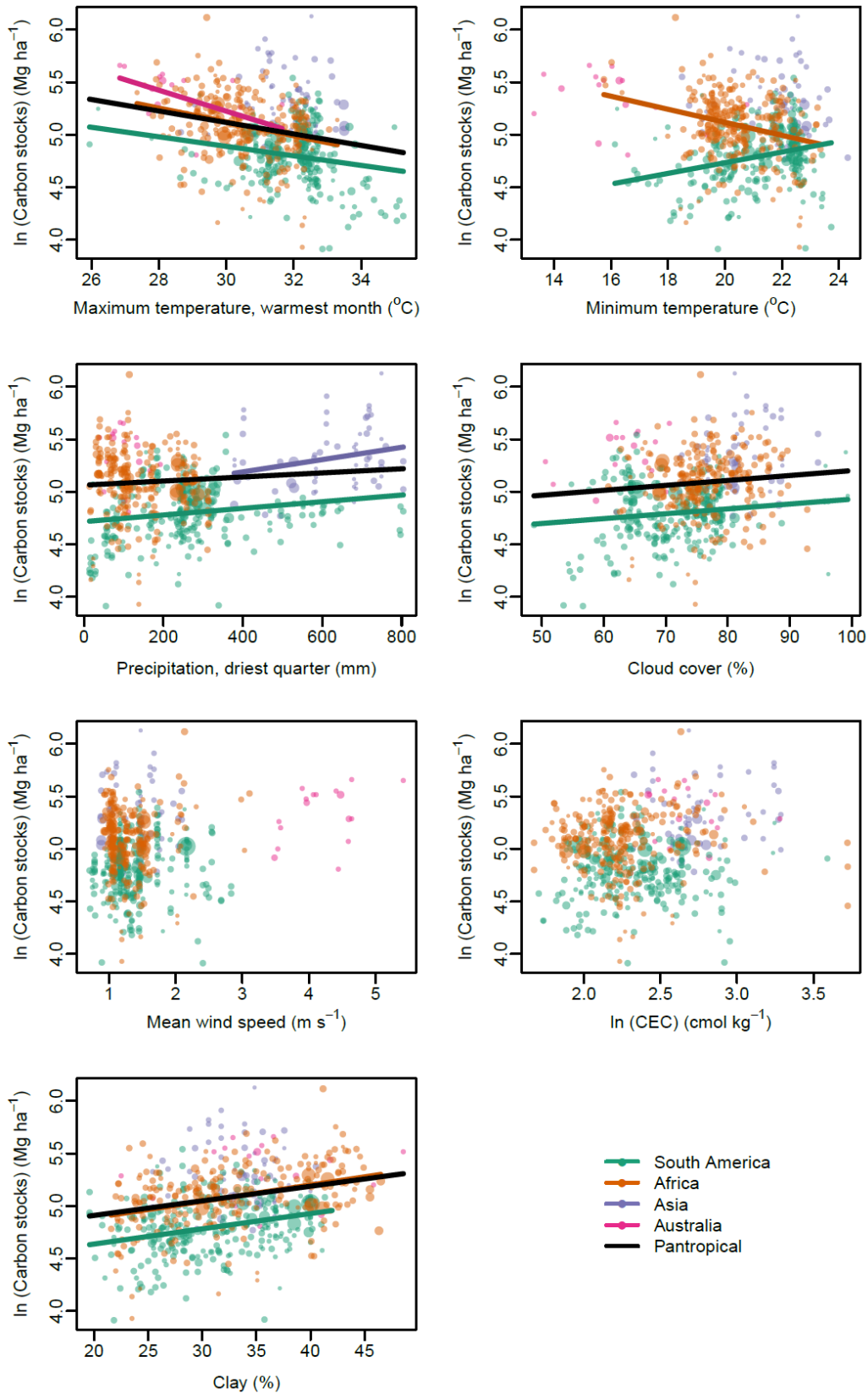
**Figure S8.** Relationships between aboveground tropical forest carbon stocks and environmental predictors. Symbols and colours as in Fig. 3. Coloured lines show bivariate relationships in each continent, and black lines show pan-tropical relationships also accounting for the effect of continent. Lines are only plotted where statistically significant.
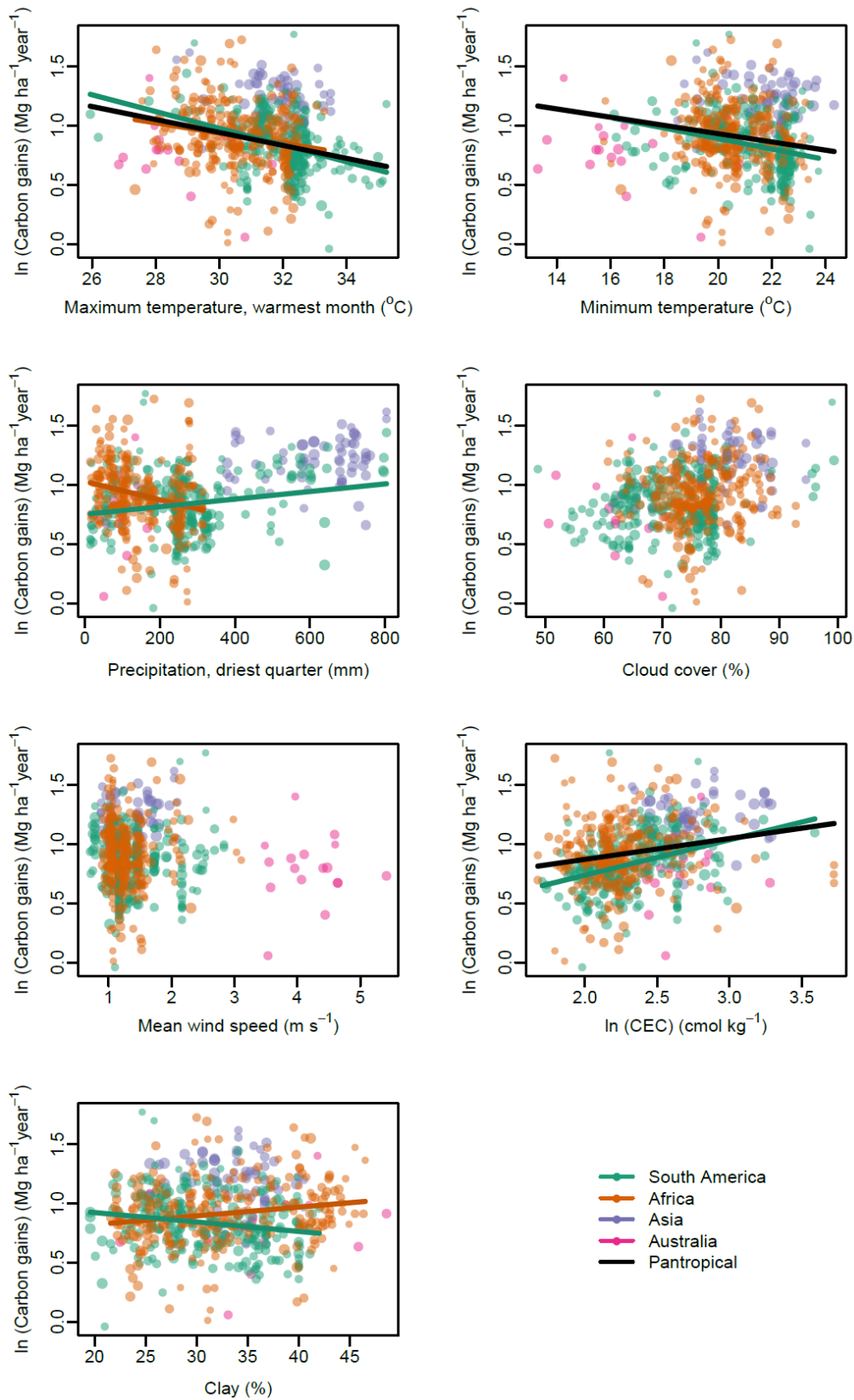
**Figure S9.** As Fig. S8, but showing relationships with carbon gains.

946

947

948

7
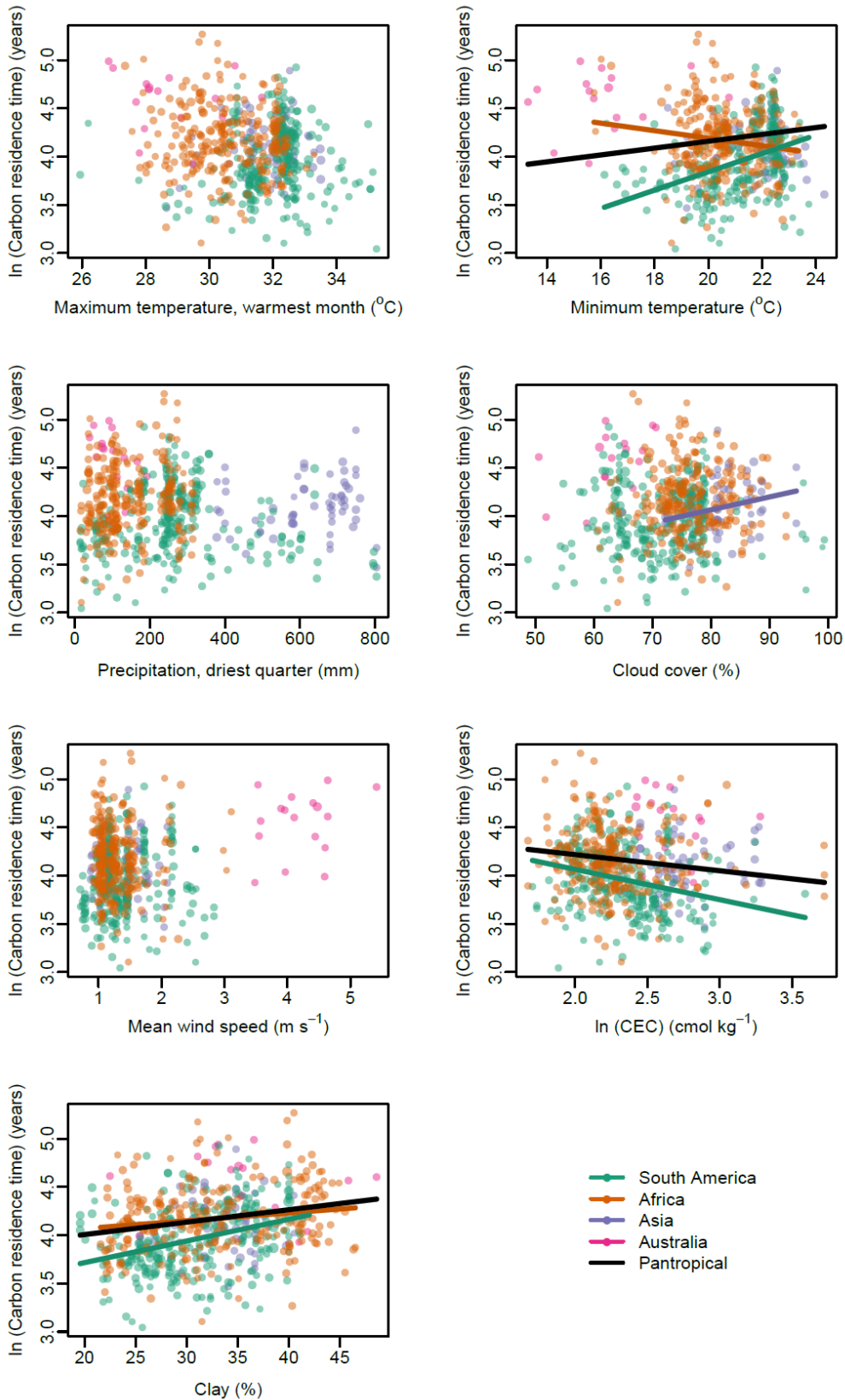
949

950    **Figure S10.** As Fig. S8, but showing relationships with carbon residence time.

951

8
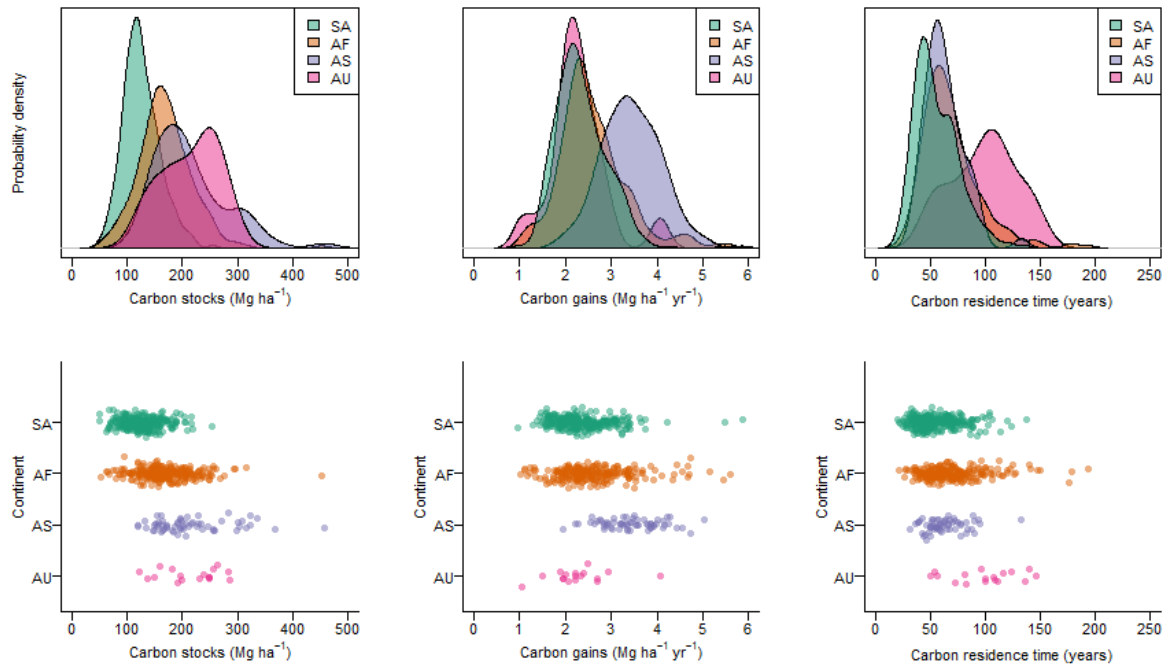
**Figure S11.** Variation in tropical forest aboveground carbon stocks, gains and residence time within and amongst continents. Data are presented as empirical probability density functions (top row) and dot-plots showing raw data points for all our multi-census plots (bottom row). SA = South America, AF = Africa, AS = Asia, AU = Australia.

## Δ Carbon stocks (Mg ha$^{-1}$)



958
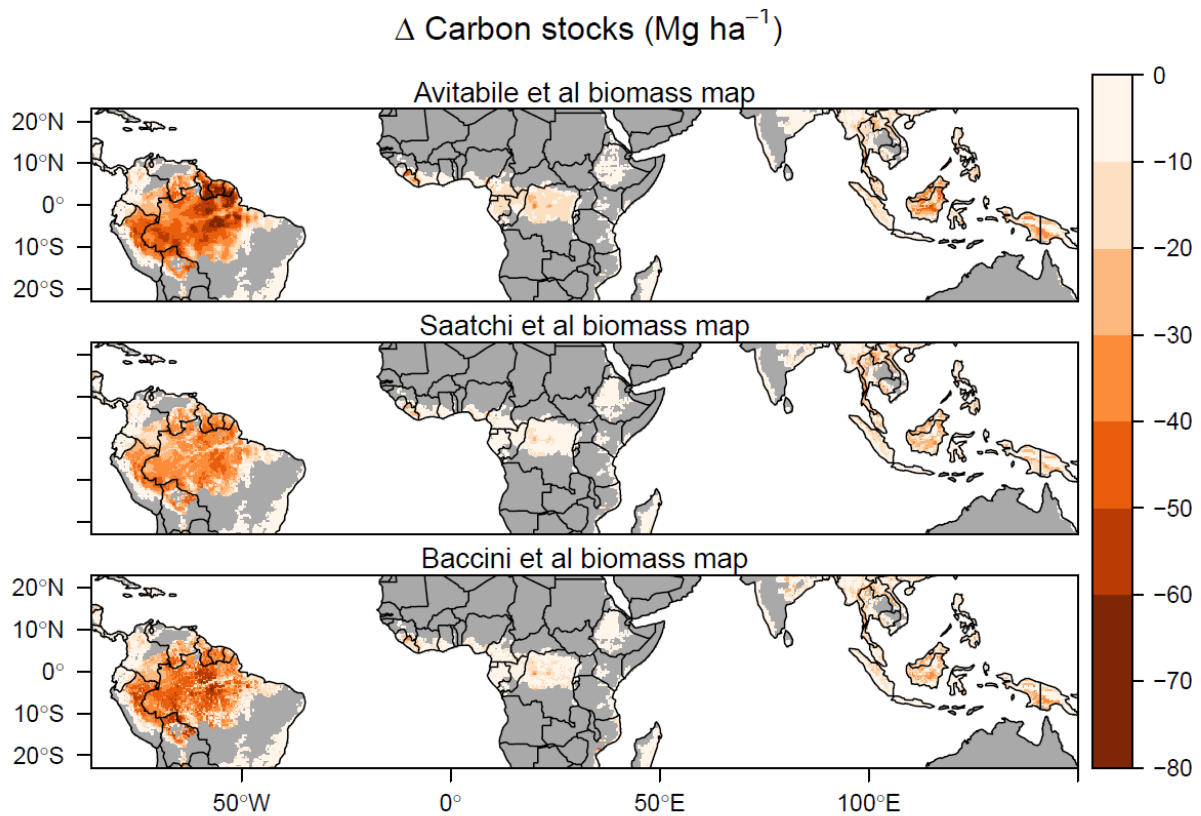
**Figure S12.** Effect of using earlier biomass reference maps for estimates of change in long-term carbon stocks for global temperature increases of ~2°C. Using aboveground biomass stock maps from Saatchi et al. (*64*) and Baccini et al. (*65*) predicted biome-wide reductions in biomass carbon stocks are 24.0 Pg (95 % CI = 5.8 – 39.6) and 28.4 Pg (95 % CI = 16.1 – 37.5) respectively. Under the ~ 1.5°C warming scenario these are 18.4 Pg (5.8 – 30.5) and 21.1 Pg (10.2 – 29.4) respectively. Results in the main text use the 2016 Avitabile et al. baseline map (*30*) – see methods for justification.

965

10

966

967
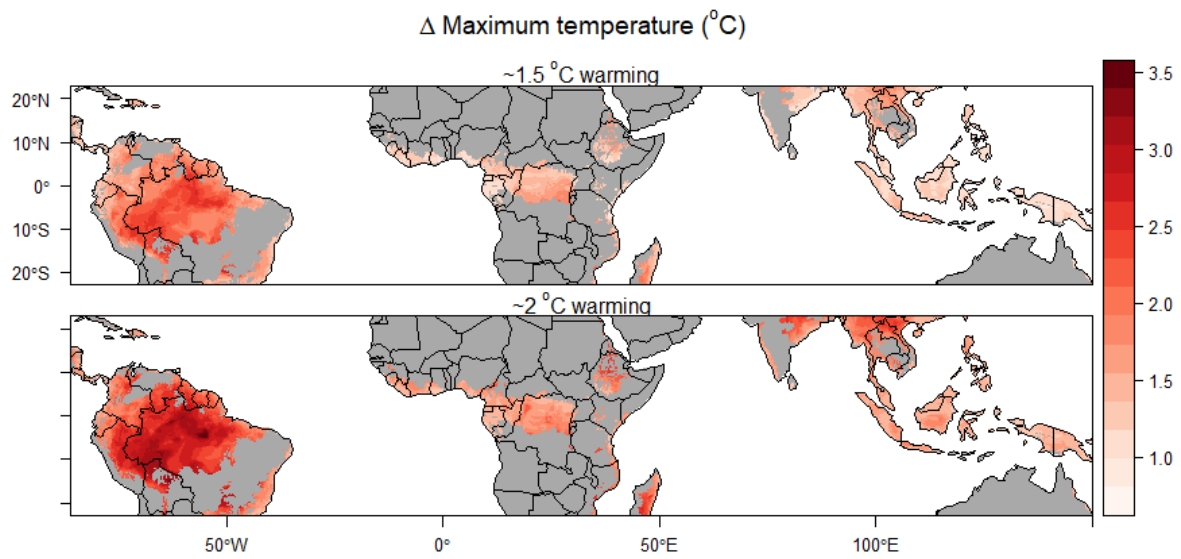


968

969  **Figure S13.** Biome-wide change in mean daily maximum temperature in the warmest month from
970  present conditions (based on the Worldclim climatology, 1970-2000), given global increases in
971  temperature of approximately 1.5°C and 2°C above pre-industrial levels. These levels of global
972  temperature increase are obtained from, respectively, RCP 2.6, 2040-2060 and RCP 4.5, 2040-2060 to
973  represent the potential spatial pattern of warming associated with global temperatures stabilising at
974  these levels. Global temperature increases of 1.5 and 2°C above pre-industrial levels (so ~0.8 °C and
975  ~1.3 °C above our current baseline climate) would lead to mean increases in maximum temperature in
976  the warmest month across the tropical forest biome of 1.9°C and 2.4°C the current baseline climate
977  respectively.

978

979

980
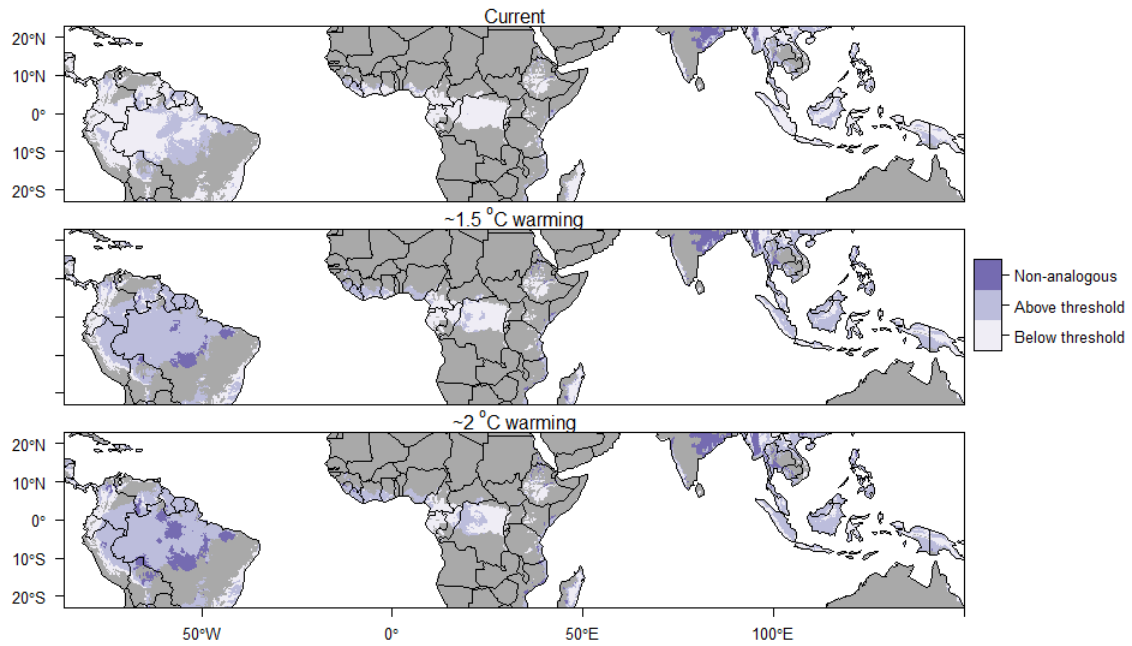


981

982 **Figure S14** Areas of the biome above or below the 32.2°C threshold, above which carbon stocks
983 decline more rapidly with temperature, under current conditions and two warming scenarios (see Fig.
984 4). Areas warmer than any currently observed in our dataset (35.2°C) are also shown (non-analogous
985 conditions). Note that even the 1.5°C warming scenario pushes most South American forests above
986 the 32.2°C threshold.

987

988

989

990

991

992



993
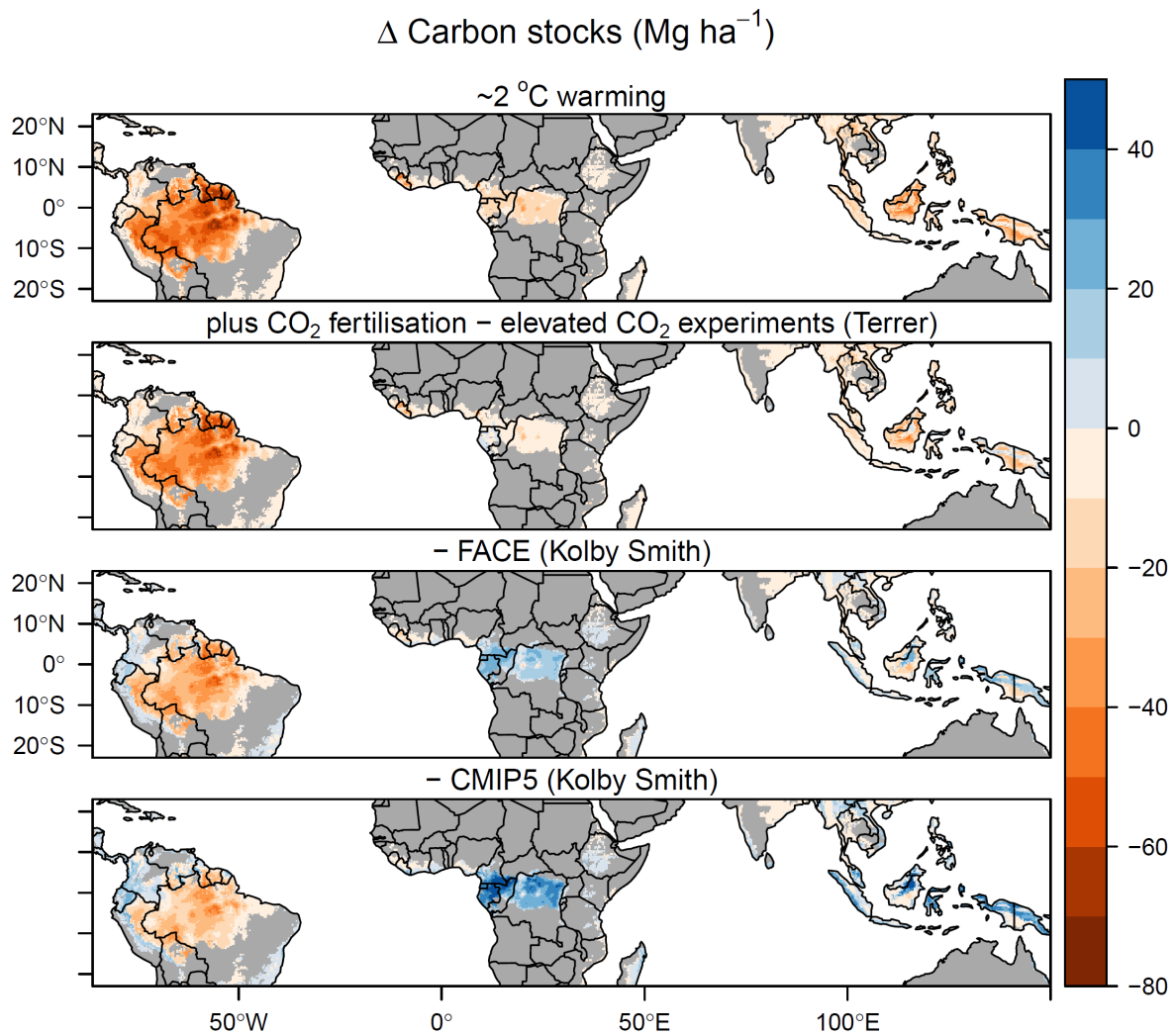
**Figure S15.** Predicted long-term change in aboveground carbon stocks under ~ 2°C global warming, based on either temperature effects alone or when also accounting for carbon dioxide growth stimulation. $CO_2$ fertilisation effects on equilibrium biomass levels were obtained from a recent synthesis of results of elevated $CO_2$ experiments (Terrer et al. (*76*)), free-air $CO_2$ enrichment (FACE) experiments (Kolby Smith et al. (*73*)) and CMIP5 earth system models (Kolby Smith et al. (*73*)). Depending on their strength, $CO_2$ effects either partially or fully ameliorate the biome-wide negative effects of increasing temperatures on biomass carbon stocks (Table S3), but these carbon stocks are predicted to decline over much of Amazonia even under the strongest $CO_2$ effect considered.

1002

1003

13

1004    **Table S1.** Climate variables selected for analysis and mechanisms by which they can affect carbon stocks.

| Climate property | Variable selected for analysis | Mechanism to affect carbon stocks |
|---|---|---|
| Daytime temperature | Maximum temperature in the warmest month[1] | High daytime temperatures exceed photosynthesis optima (*82*), increase evaporative stress, causing stomatal closure and reducing time for photosynthesis (*26*) and increase risk of mortality through hydraulic failure and/or carbon starvation (*23*). |
| Night-time temperature | Mean daily minimum temperature | Respiration rate increases with temperature so proportion of carbon taken through photosynthesis that is allocated to wood should decline with temperature (*83*). Increased respiration cost could also reduce tree longevity (*23*). As respiration occurs day and night, and photosynthesis only in the day, nighttime temperature should better reflect respiration effects and daytime temperature better reflect photosynthesis effects. |
| Moisture availability | Precipitation in the driest quarter[2] | Moisture availability could limit photosynthesis and hence carbon gains, with stomata closing when moisture availability is limiting. The risk of mortality through hydraulic failure or carbon starvation is higher when moisture is limiting (*23*), and this could also set a limit on potential tree size and hence tree longevity. |
| Light availability | Cloud frequency | Increased photosynthesis and hence AGWP when light availability is greatest (i.e. cloud cover is low) (*84*). Alternatively, light availability could have a negative effect due to high evapotranspiration stress when cloud cover is low. |
| Wind speed | Mean wind speed | Carbon stocks are expected to be lower where physical damage through wind throw or breakage is higher, as carbon is removed more quickly from the system through mortality (*85*). But there is potential for greater carbon gains if forests are more dynamic. |

1005
1006
1007    [1] Mean daily temperature in the warmest month (bio5) was selected instead of mean daily maximum temperature as it was more strongly decoupled from other climate variables. VPD could also represent some of these effects, but was too strongly correlation with maximum temperature to include as an independent variable.

1008
1009    [2] Moisture availability could also be represented by MCWD (maximum cumulative water deficit) or total precipitation, but only one of the three variables could be included in the model due to collinearity. MCWD was excluded as it is zero truncated, so less amenable to regression fitting.

1010

1

1011 **Table S2.** Coefficients of model-averaged general linear models of carbon stocks, gains and residence time as a function of climate, soil, continent and spatial
1012 autocorrelation. Coefficients are AIC weighted averages across models with $\Delta$AIC < 4 from the best performing model; variables are given a score of zero if
1013 they did not appear in a model. NA indicates that a term did not occur in any model in this set. MEM1-8 are spatial eigenvectors.

| | Carbon stocks | | | | Carbon gains | | | | Carbon residence time | | | |
|---|---|---|---|---|---|---|---|---|---|---|---|---|
| Variable | Estimate | SE | Z | P | Estimate | SE | Z | P | Estimate | SE | Z | P |
| Intercept - Africa | 4.986 | 0.010 | 476.9 | <0.001 | 0.571 | 0.525 | 1.09 | 0.278 | 3.909 | 0.688 | 5.67 | <0.001 |
| Minimum temperature | 0.031 | 0.019 | 1.67 | 0.096 | -0.001 | 0.007 | 0.18 | 0.861 | 0.019 | 0.022 | 0.88 | 0.381 |
| Maximum temperature, warmest month | -0.089 | 0.022 | 4.11 | <0.001 | -0.060 | 0.017 | 3.47 | <0.001 | -0.001 | 0.015 | 0.10 | 0.924 |
| Precipitation, driest quarter | 0.045 | 0.018 | 2.54 | 0.011 | -0.001 | 0.008 | 0.14 | 0.887 | 0.061 | 0.023 | 2.70 | 0.007 |
| Cloud frequency | 0.002 | 0.008 | 0.24 | 0.814 | -0.006 | 0.011 | 0.54 | 0.592 | 0.025 | 0.021 | 1.17 | 0.241 |
| Wind speed | 0.004 | 0.012 | 0.38 | 0.705 | 0.016 | 0.020 | 0.78 | 0.437 | -0.004 | 0.015 | 0.24 | 0.807 |
| Soil texture (% clay) | 0.021 | 0.017 | 1.26 | 0.208 | -0.005 | 0.011 | 0.49 | 0.628 | 0.040 | 0.018 | 2.17 | 0.030 |
| Soil fertility (CEC) | -0.003 | 0.009 | 0.34 | 0.732 | 0.005 | 0.011 | 0.51 | 0.613 | -0.012 | 0.017 | 0.70 | 0.486 |
| MEM1 | 0.115 | 0.014 | 7.96 | <0.001 | 0.319 | 0.559 | 0.57 | 0.569 | 0.375 | 0.734 | 0.51 | 0.610 |
| MEM2 | 0.098 | 0.017 | 5.67 | <0.001 | 0.083 | 0.273 | 0.30 | 0.762 | 0.286 | 0.359 | 0.80 | 0.427 |
| MEM3 | -0.025 | 0.014 | 1.84 | 0.065 | 0.014 | 0.041 | 0.34 | 0.735 | 0.007 | 0.054 | 0.12 | 0.904 |
| MEM4 | -0.021 | 0.011 | 1.84 | 0.066 | -0.038 | 0.020 | 1.84 | 0.066 | -0.002 | 0.027 | 0.07 | 0.945 |
| MEM5 | 0.027 | 0.011 | 2.46 | 0.014 | 0.020 | 0.015 | 1.33 | 0.182 | 0.020 | 0.020 | 0.98 | 0.327 |
| MEM6 | 0.017 | 0.011 | 1.56 | 0.118 | 0.025 | 0.011 | 2.34 | 0.019 | -0.014 | 0.014 | 1.05 | 0.293 |
| MEM7 | 0.010 | 0.011 | 0.93 | 0.353 | -0.017 | 0.010 | 1.61 | 0.107 | 0.036 | 0.014 | 2.57 | 0.010 |
| MEM8 | -0.072 | 0.013 | 5.64 | <0.001 | 0.057 | 0.012 | 4.91 | <0.001 | -0.127 | 0.016 | 7.80 | 0.000 |
| Asia | NA | | | | 0.380 | 0.542 | 0.70 | 0.485 | -0.753 | 0.683 | 1.10 | 0.271 |
| Australia | NA | | | | -0.173 | 0.390 | 0.44 | 0.658 | 0.006 | 0.516 | 0.01 | 0.990 |
| South America | NA | | | | 0.643 | 1.164 | 0.55 | 0.582 | 0.542 | 1.530 | 0.35 | 0.724 |

1014

2

1015  **Table S3.** Predicted biome-wide changes in long-term biomass carbon stocks (scaled to include root
1016  biomass) under global temperature increases of ~ 1.5°C and ~ 2°C. Changes are based on temperature
1017  effects alone, and when also accounting for the effect of increased $CO_2$ concentrations on tree growth.
1018  $CO_2$ effects were obtained from a synthesis of results of elevated $CO_2$ experiments (Terrer et al. (*76*)),
1019  free-air $CO_2$ enrichment (FACE) experiments (Kolby Smith et al. (*73*)) and CMIP5 earth system
1020  models (Kolby Smith et al. (*73*)). 95% confidence intervals around changes (based on uncertainties in
1021  temperature effects alone) are shown in parentheses.

| $CO_2$ effect | Change in biomass carbon stocks (Pg) | |
| --- | --- | --- |
| | ~ 1.5°C warming (443 ppm $CO_2$) | ~ 2°C warming (487 ppm $CO_2$) |
| None | -26.9 (-38.4 - -15.8) | -35.3 (-49.0 - -20.9) |
| Terrer et al. elevated $CO_2$ experiments | -22.0 (-33.0 - -9.9) | -26.3 (-37.6 - -11.5) |
| Kolby Smith et al. FACE experiments | -6.2 (-16.8 – 7.7) | -9.9 (-24.3 – 3.9) |
| Kolby Smith et al. CMIP5 models | 3.9 (-8.3 – 12.6) | 2.0 (-11.9 – 19.8) |

1022